ACS ENGINEERING Au
AN OPEN ACCESS JOURNAL OF THE AMERICAN CHEMICAL SOCIETY

pubs.acs.org/engineeringau
Article

Photocurable Adhesive Composed of Modified Castor Oil and Enhanced by Valorized Glycerol from Waste Cooking Oil

Vojtěch Jašek,* Otakar Bartoš, Jan Prokeš, Eliška Kameníková, Radek Přikryl, and Silvestr Figalla

Cite This: ACS Eng. Au 2026, 6, 142−158
Read Online

ACCESS | Metrics & More | Article Recommendations | Supporting Information

ABSTRACT: This article describes the production of a photocurable adhesive from renewable sources, i.e., castor oil and waste cooking oil. An innovative castor oil ethanolamide methacrylate (Oil-EA-Met) was synthesized to form the primary binder precursor. The waste-oil-resourced glycerol derivatives, modified to mono-, di-, and trimethacrylate derivatives (MGLY, DGLY, and TGLY), represent functional additives. All products were cross-analyzed using ^{1}H NMR, ESI-MS, FTIR, and GC-FID. Oil-EA-Met represented 75% of the formulated precursor systems, while the functional additive (MGLY, DGLY, TGLY, and a commercially available 2-hydroxyethyl methacrylate (HEMA)) represented 25% of the curable precursor. MGLY had the best impact on the adhesion performance. This additive exhibited the highest polymerization reactivity (E_a = 68.2 kJ/mol), a complete miscibility with water, the highest thermal resistivity, a thermomechanical profile, a flexural character, and the highest ISO 2049 adhesion levels on wood−glass substrates (reaching level 5 (the highest)) and wood−PMMA substrates (level 3). The adhesive containing MGLY reached a similar wood−glass adhesion shear strength of 1400 kPa as the system with HEMA and surpassed the HEMA system for the wood−PMMA system (the MGLY system reached 800 MPa; the HEMA system achieved 530 MPa).

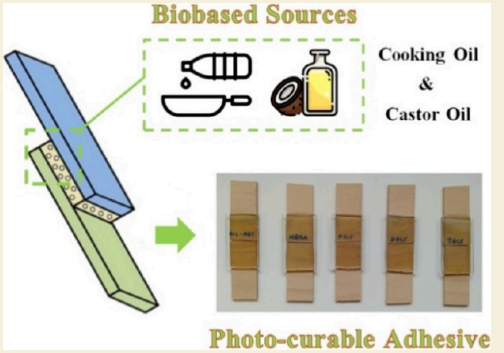

KEYWORDS: *castor oil, aminolysis, waste oil, transesterification, glycerol, Esterification, Adhesives*

1. INTRODUCTION

Photocurable adhesives for connecting various substrates, such as amorphous polymers (acrylic or PTFE), glass, metal, or wood, are currently extensively investigated due to their application efficiency ensured by a fast and direct curability.[1,2] Since the photoinitiated curability requires a transparent matrix to be involved in the application, especially translucent materials are ideal candidates for these adhesives.[3] The target material's chemical composition is crucial for the ideal curable precursor suggestion. Many transparent hydrophobic matrices require specific nonpolar reactive precursors to perform optimally during adhesion.[4] Materials such as poly(methyl methacrylate) (PMMA),[5] poly(ethylene terephthalate) (PET),[6] poly(tetrafluoroethylene) (PTFE),[7] and poly(carbonate) (PC)[8] exhibit a primarily hydrophobic character and comprise long saturated carbon chains and mainly nonpolar functional groups. Several polar and hydrophilic substrates, namely, glass or wood materials, require different adhesive precursors that fulfill their working role effectively.[7,9,10] Glass is composed primarily of silica (SiO_2), forming tetrahedral structures involving Na^+ or Ca^{2+} ions within the molecular arrangement.[13] Si−O bonds and atomic ions exhibit a strong hydrophilic character, which has to be reflected in the applied adhesive.[11,12] Wood comprises multiple organic polymers: cellulose, hemicellulose, and lignin.[14] These biomacromolecules contain many polar functional groups (hydroxyl, esters, carbonyls, and ethers), which increase the surface energy of the system, affecting the eventual strong hydrophilic character.[15] The adhesives engineered for different substrates usually possess a similar chemical character to the target matrices to maximize functional performance.

Numerous commercial adhesives serve various target substrates such as cyanoacrylates, polyurethanes, epoxides, or reactive multicomponent acrylic binders.[16] Many of the listed adhesives suffer from several inconveniences related to the chemical foundation of their function. Polyurethane (PU) adhesives typically require a long cure time (up to 16 h at elevated temperature), and their applicability is limited due to the storage at decreased temperatures (4−25 °C).[17] Additionally, PU adhesives consist of two separate components, complicating the application process.[18] Epoxy adhesives also contain multiple working components, and their complete cure requires up to 24 h.[19] Acrylate and cyanoacrylate adhesives are the most universal, use-efficient, and monocomponent systems for glue applications.[20,21] Particularly polar substrates work

Received: September 30, 2025
Revised: November 11, 2025
Accepted: November 12, 2025
Published: November 19, 2025

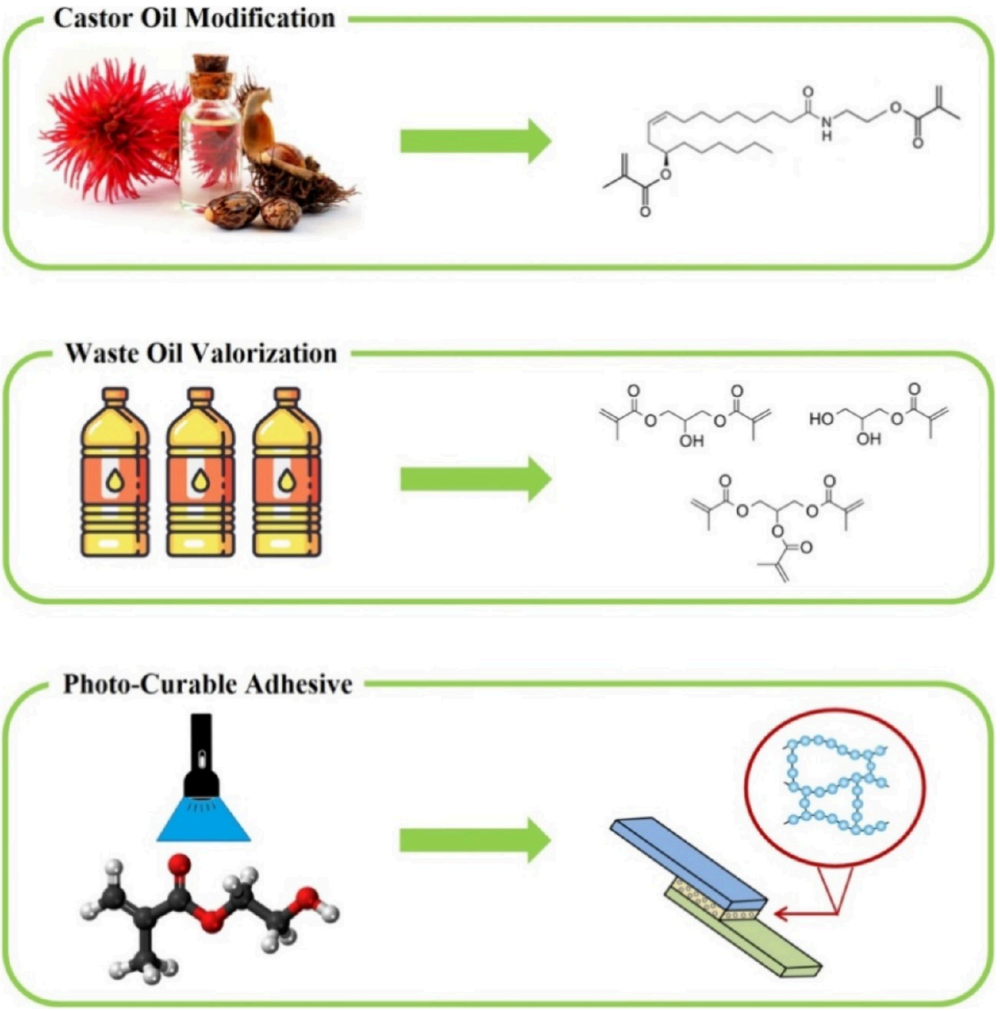

Figure 1. Summarized steps involving castor oil modification and waste cooking oil valorization toward the production of photocurable adhesives.

effectively with silicone adhesives due to their polar molecular character, which provides optimal affinity for the hydrophilic materials.[22] Wood materials also work effectively with contact adhesives. Widely used contact glues comprise solubilized poly(vinyl acetate) (PVAc),[23] poly(vinyl alcohol) (PVA),[24] or suspended starch.[25] These adhesives exhibit sufficient polarity to connect substrates with high surface energy.

Biobased entering compounds play a significant role in current adhesive development. Sustainability and resource diversity in this segment are increasing due to the legislative regulations (particularly in the European Union), and the users in specific segments also demand more green and renewable reactants to work with.[26,27] Regarding the sources with the biggest perspective, vegetable oils,[27] natural polyesters,[28] and biobased acrylates/methacrylates[29] are often studied as suitable adhesive precursors. Triacylglycerides are used as coatings and adhesives regularly in the form of alkyds[30] or fatty acid dimers.[31] Their hydrophobic character is exhibited through long hydrocarbon chains possessing a strong hydrophobic character;[27,30,31] therefore, several chemical modifications are projected into their structure to improve their performance, such as hydroxylation, epoxidization, or acylation.[27,44] The unsaturated double bonds must be present in the particular oil's structure since they are the reactive functional group capable of modification.[32] Acrylated and methacrylated oils are some of the most widely used triacylglyceride derivatives produced from epoxidized precursors. These systems allow the UV/vis curing approach to obtain highly curable, biobased precursors as a suitable adhesive for numerous substrates.[33,34] Typically, the acrylated and methacrylated oils comprise free hydroxyl groups formed during the modification, which increase the adhesion toward several materials.[35,36] The same types of radically polymerized adhesives are obtained from the application of itaconic acid (IA) derivatives.[37] IA is a reactive compound from renewable sources that ensures the entirely natural fabrication of adhesives.[39] Commonly, the applicability of IA involves its modification into esters since this natural dicarboxylic acid has a melting point of 162−164 °C,[38] prohibiting its direct usage as a liquid adhesive precursor.[7]

The optimal coating potential based on the multiple polar and functional groups, such as amine, *N*-acetyl, ester, and hydroxyl, was investigated in numerous papers. The highly biobased entering reactants obtained from potentially waste sources are chitosan or rosin acids from the tree rosin. Chitosan can form a physically cross-linked structure that is optimal for the formation of thin layers. The rosin derivatives served as an additional cross-linking component. In the combination, the highly performing natural coatings were formed and applied to the wood substrates.[71] Other amine-containing compounds based on polydopamine (PDA) were experimentally tested for adhesive and membrane-forming purposes.[72] The well-known hydrogels based on poly(ethylene

https://doi.org/10.1021/acsengineeringau.5c00084
ACS Eng. Au 2026, 6, 142−158

glycol) methacrylate (PEGMA), enriched with L-serine and glycerol, were investigated for sand stabilization purposes. The rapid fast soaking is their key property determining their utility. The exceptional hydrophilic character was provided by numerous free hydroxyl groups from the present glycerol and the carboxyl and amine bonding present in L-serine.[73]

This presented work introduces an innovative castor oil derivative, the polymerizable castor oil ethanolamide, which is produced via catalystless synthesis at mild reaction conditions (100 °C, 300 min). This highly biobased intermediate was activated via methacrylic anhydride (MAAH) to form a curable thermoset precursor possessing multiple polar functional groups (ester, amide). After the modification, the formed secondary product, methacrylic acid (MA), was quantitatively distilled to serve as the continuous species for methacrylation via Fischer esterification of the obtained glycerol from waste cooking oil. The valorized glycerol was converted into mono/di/tri esterified precursors (MGLY: glycerol monomethacrylate, DGLY: glycerol dimethacrylate, and TGLY: glycerol trimethacrylate). This multiple-step approach uses all reactive carboxylic substances, avoiding disposal generation and maximizing the added-value products. The synthesized compounds were cross-analyzed by ^{1}H NMR, ESI-MS, FTIR, and GC-FID. The reactivity and following applicability of the formed thermoset-forming precursors in the adhesion field were investigated in detail in this article. The experiments and approaches performed are summarized in Figure 1.

2. EXPERIMENTAL SECTION

2.1. Materials

The castor oil (hydroxyl value of 154 mg KOH/g) was purchased from Fichema Ltd. (Czech Republic). The waste cooking oil was kindly obtained from the local cafeteria (initial acidity = 4 mg KOH/g) (Czech Republic). Ethanolamine (99%, p.a.), methanol (99% p.a.), potassium hydroxide (99%, p.a.), potassium acetate (99%, p.a.), sulfuric acid (98%), sodium sulfate (99%, anhydrous), and ethyl acetate (99%, p.a.) were purchased from Penta Ltd. (Czech Republic). Methacrylic anhydride (98%), BAPO (photoinitiator, phenylbis(2,4,6-trimethylbenzoyl)phosphine oxide, 98%), Luperox DI (thermal initiator for the reactivity study, *tert*-butyl peroxide, 99%), D-chloroform (solvent for NMR analyses, $CDCl_3$), methacrylic acid (99%), and 2-hydroxyethyl methacrylate (97%) were obtained from Sigma-Aldrich (Merck, Germany).

2.2. Structure Verification Methods

Nuclear magnetic resonance (NMR) was applied to obtain ^{1}H spectra to confirm the structural identity of the synthesized compounds. The measurements were conducted using a Bruker Avance III 500 MHz (Bruker, Billerica, MA, USA). The measuring frequency was 500 MHz for ^{1}H NMR. The measurements were performed at 30 °C temperature using D-chloroform ($CDCl_3$) as a solvent with tetramethylsilane (TMS) as an internal standard. The chemical shifts (δ) are expressed in parts per million (ppm) units, referenced by a solvent. The coupling constant (J) is expressed with frequency unit (Hz), with coupling expressed as s: singlet, d: doublet, t: triplet, q: quartet, p: quintet, and m: multiplet.

Electrospray mass spectrometry (ESI-MS) contributed to the structural cross-analysis of the synthesized compounds. We used Bruker EVOQ LC-TQ instrumentation for the measurements. Product scan spectra were obtained by fragmentation of the following molecular precursor ions ($[M + H]^+$, $[M - H_2O + H]^+$, and $[M - H]^-$), detailed in the synthesis section for every produced compound. Collision energy spread (5−20 eV) improved the collected MS/MS data quality. Furthermore, the obtained mass spectra agree with their in silico prediction by CFM-ID 4.0,[40] which also proposed the product ion structure for the most intense masses.

Fourier-transform infrared spectroscopy (FTIR) was a structural confirmation method to detect specific functional groups within the synthesized compounds' structures. Analyses were performed using a Bruker Tensor 27 (Billerica, MA, USA) and the attenuated total reflectance (ATR) method. Diamond served as the dispersion component. A diode laser was the irradiation source in this spectroscope. The Michelson interferometer was used to quantify the signal. Spectra comprised 32 total scans with a measurement resolution of 2 cm^{-1}. According to the previously published FTIR-based method,[41] we used the double bond conversion calculation. The calculation is displayed in eq 1:[41]

$$\text{conversion} = \left(1 - \frac{\left(\frac{A_{C=C}}{A_{C=O}}\right)_{\text{cured}}}{\left(\frac{A_{C=C}}{A_{C=O}}\right)_{\text{uncured}}}\right) \times 100 \quad (1)$$

where the conversion (%) is calculated from following parameters: $A_{C=C}$ is the integral area of the vinyl C=C bending signal (−), and $A_{C=O}$ is the integral area of the C=O stretching signal of ester (−). We used the C=C bending signal instead of the stretching signal due to the presence of the amide signal in the same wavenumber interval as the C=C stretching signal.

Castor oil derivatives were analyzed by standardized hydroxyl value measurement (DIN EN ISO 4629-2).

Gas chromatography (GC) (Hewlett-Packard 5890 Series II) with a flame ionization detector (FID) contributed to structural confirmation. Nitrogen (as an auxiliary gas for FID), air (as an oxidizer for FID), and hydrogen (as a carrier gas and fuel for FID) gases were used. The capillary GC column ZB-624 (60 m × 0.32 mm, 1.8 μm) served as a stationary phase. The temperature of the inlet was set to 280 °C, and the temperature of the detector was set to 280 °C. Substances were separated with a temperature gradient, with an initial temperature of 120 °C (held for 1 min) followed by a temperature rate of 15 °C/min with a final temperature of 250 °C (held for 8 min). The column flow rate set for the analyses was 3 mL/min, and the split ratio was 1:40. The injection volume applied in all analyses was 1 μL (1 wt % sample solution in tetrahydrofuran (THF)).

We included a three-point flexural test to investigate the mechanical properties of the prepared cured thermosets. We prepared Oil-EA-Met-based systems containing 25 wt % of the synthesized compounds (MGLY, DGLY, and TGLY) and the reference (HEMA). BAPO (photoinitiator) was mixed into the systems (1 wt %), and the precursors were cured by an irradiation source of 405 nm wavelength and 990 mW/m^2 of the irradiation power for 90 min (to ensure the complete polymerization). The rectangular specimens had dimensions of 80 × 10 × 4 mm according to the CSN EN ISO 178 standard (by which the test was conducted). The loading nose and support radius were 5 mm with a support span of 64 mm. The test speed was set to 10 mm·min^{-1}.

The thermomechanical properties were investigated by a DMA 2980 from TA Instruments (New Castle, DE, USA). The tested objects had the following parameters: 50 × 10 × 4 mm. Objects were applied to a dual cantilever attachment, and the parameters of applied deformation were 25 μm amplitude and 1 Hz frequency. The temperature increased from 30 to 120 °C at a rate of 3 °C/min. The storage modulus, loss modulus, and tan δ values were obtained directly from DMA analysis.

Thermogravimetric analysis (TGA) provided information regarding the heat-resistance properties. We used the formed thermosets for mechanical and DMA analysis. TGA was performed on a TGA Q500 from TA Instruments (New Castle, DE, USA). The degradation process of a sample (10−15 mg) was monitored via the following heating conditions: equilibration at 40 °C, heating to 600 °C at a heating rate of 10 °C/min under N_2, and 10 min at 600 °C under an air atmosphere. The heat-resistant index was obtained from the proposed eq 2:[41]

$$T_s = 0.49[T_5 + 0.6(T_{30} - T_5)] \quad (2)$$

https://doi.org/10.1021/acsengineeringau.5c00084
ACS Eng. Au 2026, 6, 142−158

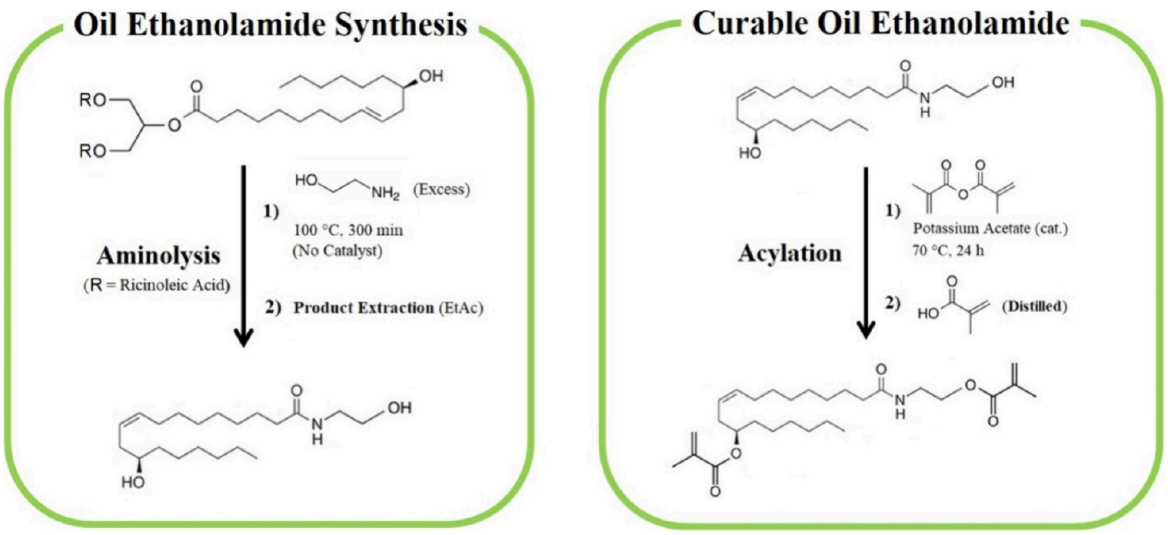

Figure 2. Reaction scheme of the castor oil modification into castor oil ethanolamide (Oil-EA) and castor oil ethanolamide methacrylate (Oil-EA-Met).

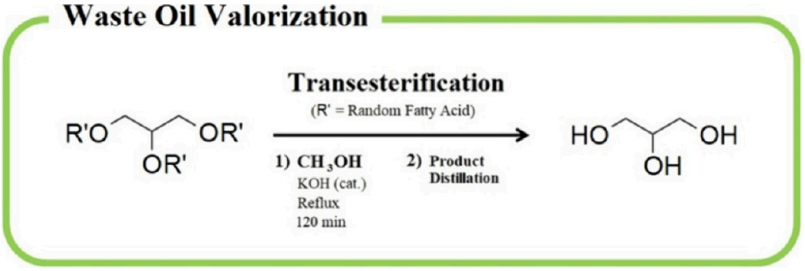

Figure 3. Reaction scheme of waste cooking oil transesterification forming glycerol for further modification to curable precursors.

where T_s is the heat-resistant index (−), T_5 refers to the temperature at 5% of mass loss (°C), and T_{30} is the temperature at 30% of mass loss (°C).

2.3. Synthesis of the Castor Oil Curable Derivative

Castor oil (310 g, 0.33 equiv) was introduced into a round-bottom flask with ethanolamine (181 g, 3.0 equiv). The reaction mixture was set into an oil bath and tempered at 100 °C for 300 min (see Figure 2, left). After the reaction time, the solution was mixed with ethyl acetate (1:1 volume ratio) and washed with water twice to remove excess ethanolamine. The organic phase was separated, and the solvent was evaporated. The obtained castor oil ethanolamide (Oil-EA) was cross-analyzed.

The formed Oil-EA (300 g, 0.88 equiv) was mixed with methacrylic anhydride (MAAH, 271 g, 1.8 equiv) and potassium acetate (catalyst, 0.98 g, 0.01 equiv), and the reaction mixture was set to 70 °C in an oil bath for 24 h (see Figure 2, right). After the reaction time, the formed secondary product, methacrylic acid (MA), was distilled at reduced pressure (75 Torr) at 100 °C with continuous airflow (20 mL of air per minute), which increased the volatility of MA and inhibited its polymerization. After the distillation, the catalyst and the residual MA were extracted with water once. The purified product, castor oil ethanoamide methacrylate (Oil-EA-Met), was dried over anhydrous sodium sulfate and cross-analyzed.

2.3.1. Castor Oil Ethanolamide (Oil-EA). ^{1}H NMR (Figure S1) (500 MHz, $CDCl_3$) δ 6.22−6.09 (m, 1H), 5.59−5.50 (m, 1H), 5.45−5.35 (m, 1H), 3.73−3.67 (m, 2H), 3.66−3.57 (m, 1H), 3.41 (td, J = 5.5, 4.2 Hz, 2H), 2.24−2.15 (m, 4H), 2.10−1.97 (m, 2H), 1.62 (q, J = 7.2 Hz, 2H), 1.46 (tdd, J = 11.4, 6.1, 3.7 Hz, 2H), 1.39−1.24 (m, 15H), 0.92−0.85 (m, 3H).

ESI-MS fragmentation spectrum (Figure S2) and ($C_{20}H_{39}NO_3$) spectrum calcd $[M + H]^+$ 342.5 m/z, found 342.0 m/z.

FTIR (Figure S3) absorption wavenumber intervals: O−H and N−H stretch 3550−3200 cm^{-1}, C−H stretch 3000−2840 cm^{-1}, C═O (amide) stretch 1690−1670 cm^{-1}, C−N stretch 1250−1020 cm^{-1}.

2.3.2. Castor Oil Ethanolamide Methacrylate (Oil-EA-Met). ^{1}H NMR (Figure S4) (500 MHz, $CDCl_3$) δ 6.27−6.05 (m, 2H), 5.84−5.79 (m, 1H), 5.79−5.53 (m, 2H), 5.56−5.30 (m, 2H), 4.28−4.22 (m, 2H), 3.65−3.50 (m, 3H), 2.24−2.12 (m, 6H), 2.09−1.89 (m, 6H), 1.60 (t, J = 6.7 Hz, 2H), 1.51−1.41 (m, 2H), 1.39−1.20 (m, 16H), 0.92−0.84 (m, 3H).

ESI-MS fragmentation spectrum (Figure S5) and ($C_{28}H_{47}NO_5$) spectrum calcd $[M + H]^+$ 478.3 m/z, found 478.2 m/z.

FTIR spectrum (Figure S6) absorption wavenumber intervals: N−H stretch 3550−3200 cm^{-1}, C−H stretch 3000−2840 cm^{-1}, C═O (ester) stretch 1750−1735 cm^{-1}, C═O (amide) stretch 1690−1670 cm^{-1}, N−H bend 1650−1580 cm^{-1}, C−N stretch 1250−1020 cm^{-1}.

2.3.3. Methacrylic Acid (MA). ^{1}H NMR (Figure S7) (500 MHz, $CDCl_3$) δ: 11.68 (s, 1H), 6.26 (dd, J = 1.5, 1.0 Hz, 1H), 5.68 (p, J = 1.6 Hz, 1H), 1.96 (dd, J = 1.6, 1.0 Hz, 3H).

ESI-MS (Figure S8) fragmentation spectrum ($C_4H_6O_2$) spectrum calcd $[M - H]^-$ 85.1 m/z, found 85.1 m/z.

FTIR spectrum (Figure S9) absorption wavenumber intervals: O−H stretch 3550−3200 cm^{-1}, C−H stretch 3000−2840 cm^{-1}, C═C stretch 1662−1626 cm^{-1}, C−O (acid) stretch 1210−1163 cm^{-1}, C═C bend 840−790 cm^{-1}.

2.4. Valorization of the Waste Cooking Oil into Curable Glycerol Derivatives

The waste cooking oil (1900 g, 2 equiv) was introduced into a 4000 mL round-bottom flask together with methanol (384 g, 12 equiv) and potassium hydroxide (5.61 g, 0.1 equiv) and refluxed in a heating nest for 120 min (see Figure 3). After the reaction time, the reaction mixture naturally separated. The fatty acid methyl esters formed were separated and could be used as a biodiesel. The glycerol phase was

https://doi.org/10.1021/acsengineeringau.5c00084
ACS Eng. Au 2026, 6, 142−158

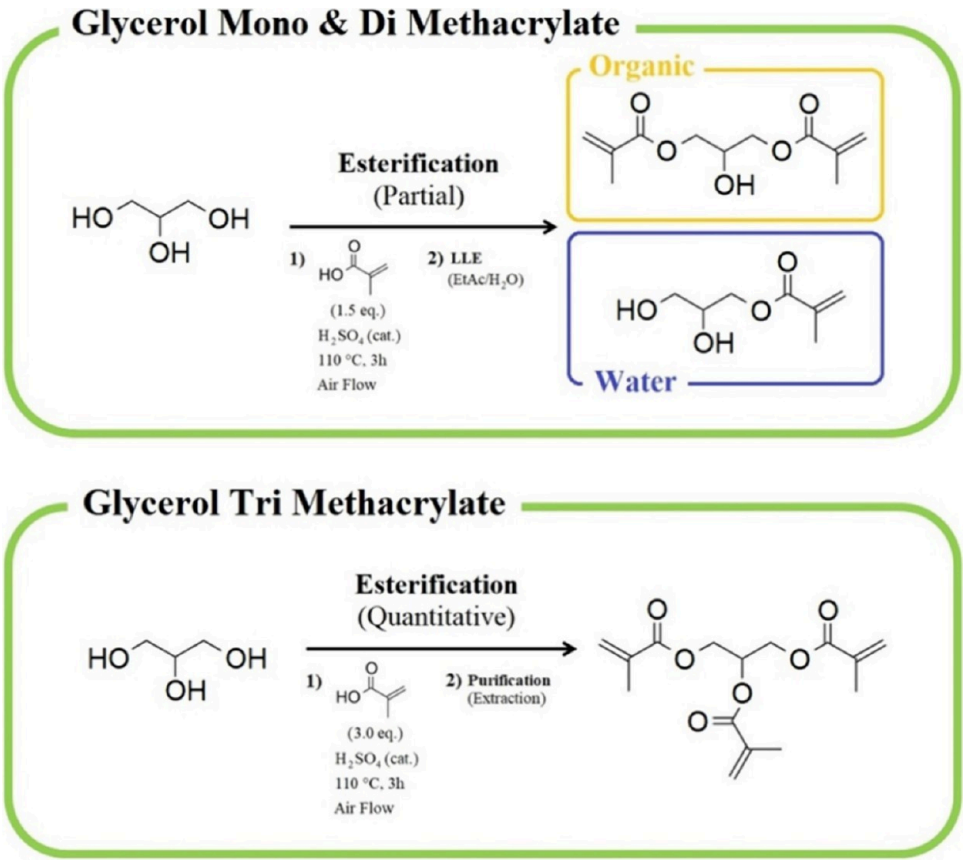

Figure 4. Reaction scheme of the valorized glycerol modification to partially methacrylated (glycerol monomethacrylate (MGLY) and dimethacrylate (DGLY)) and fully methacrylated derivatives (glycerol trimethacrylate (TGLY)).

neutralized with sulfuric acid to pH 7 and distilled at reduced pressure (10 Torr) in a heating nest. The distilled glycerol was cross-analyzed.

2.4.1. Glycerol. ^{1}H NMR (Figure S10) (500 MHz, $CDCl_3$) δ 3.86−3.79 (m, 1H), 3.77 (dd, J = 11.2, 3.8 Hz, 2H), 3.69 (dd, J = 11.3, 5.6 Hz, 2H).

FTIR spectrum (Figure S11) absorption wavenumber intervals: O−H stretch 3550−3200 cm^{-1}, C−H stretch 3000−2840 cm^{-1}, C−O stretch 1210−1163 cm^{-1}.

GC-FID determined the retention time (Figure S12) at the particular analysis parameters: 9.6 min RT.

The produced glycerol (92 g, 1 equiv) was mixed with nonquantitative (130 g, 1.5 equiv) and quantitative (260 g, 3 equiv) amounts of methacrylic acid (the produced acid was used together with additional acid) to form partially methacrylated (glycerol monomethacrylate (MGLY), glycerol dimethacrylate (DGLY)) and fully methacrylated (glycerol trimethacrylate (TGLY)) curable glycerol derivatives. Both reaction batches contained sulfuric acid (0.98 g, 0.01 equiv) as an esterification catalyst. The reaction water was quantitatively distilled at a pressure of 120 Torr and a temperature of 110 °C for 3 h. The reaction batch producing partially methacrylated glycerol (Figure 4, top) involved a liquid−liquid extraction process (LLE). The postreaction mixture was diluted with ethyl acetate (1:1 volume ratio) and mixed with water (1:1 volume ratio to the ethyl acetate diluted solution) to separate water-soluble MGLY from water-insoluble DGLY. After the LLE, both products were purified by solvent distillation. The quantitative esterification product, TGLY (Figure 4, bottom), was washed with water once to remove the catalyst from the product. The purified TGLY was dried over anhydrous sodium sulfate. All produced glycerol derivatives (MGLY, DGLY, and TGLY) were cross-analyzed.

2.4.2. Glycerol Monomethacrylate (MGLY). ^{1}H NMR (Figure S13) (500 MHz, $CDCl_3$) δ 6.15 (q, J = 1.2 Hz, 1H), 5.65−5.57 (m, 1H), 4.36−4.15 (m, 2H), 4.15−3.75 (m, 1H), 3.72−3.44 (m, 2H), 1.96 (t, J = 1.3 Hz, 3H).

ESI-MS (Figure S14) fragmentation spectrum ($C_7H_{12}O_4$) spectrum calcd $[M - H_2O + H]^+$ 143.2 m/z, found 142.9 m/z.

FTIR spectrum (Figure S15) with absorption wavenumber intervals: C−H stretch 3000−2840 cm^{-1}, C═O (ester) stretch 1750−1735 cm^{-1}, C═C stretch 1662−1626 cm^{-1}, C−O (ester) stretch 1210−1163 cm^{-1}, C═C bend 840−790 cm^{-1}.

GC-FID determined the retention time (Figure S16) at the particular analysis parameters: 10.3 min RT.

2.4.3. Glycerol Dimethacrylate (DGLY). ^{1}H NMR (Figure S17) (500 MHz, $CDCl_3$) δ 6.17−6.07 (m, 2H), 5.60 (dtd, J = 9.9, 3.3, 1.7 Hz, 2H), 4.52−3.38 (m, 5H), 1.98−1.90 (m, 6H).

ESI-MS (Figure S18) fragmentation spectrum ($C_{11}H_{16}O_5$) spectrum calcd $[M - H_2O + H]^+$ 211.2 m/z; found 210.9 m/z.

FTIR spectrum (Figure S19) with absorption wavenumber intervals: C−H stretch 3000−2840 cm^{-1}, C═O (ester) stretch 1750−1735 cm^{-1}, C═C stretch 1662−1626 cm^{-1}, C−O (ester) stretch 1210−1163 cm^{-1}, C═C bend 840−790 cm^{-1}.

GC-FID determined the retention time (Figure S20) at the particular analysis parameters: 10.7 min RT.

2.4.4. Glycerol Trimethacrylate (TGLY). ^{1}H NMR (Figure S21) (500 MHz, $CDCl_3$) δ 6.17−6.05 (m, 3H), 5.61 (dtd, J = 10.0, 3.2, 1.6 Hz, 3H), 5.44 (tt, J = 6.0, 4.4 Hz, 1H), 4.46−4.15 (m, 4H), 1.95 (dt, J = 12.7, 1.4 Hz, 9H).

ESI-MS (Figure S22) fragmentation spectrum ($C_{15}H_{20}O_6$) spectrum calcd $[M - H_2O + H]^+$ 296.3 m/z, found 296.1 m/z.

FTIR spectrum (Figure S23) with absorption wavenumber intervals: C−H stretch 3000−2840 cm^{-1}, C═O (ester) stretch 1750−1735 cm^{-1}, C═C stretch 1662−1626 cm^{-1}, C−O (ester) stretch 1210−1163 cm^{-1}, C═C bend 840−790 cm^{-1}.

GC-FID determined the retention time (Figure S24) at the particular analysis parameters: 10.2 min RT.

https://doi.org/10.1021/acsengineeringau.5c00084
ACS Eng. Au 2026, 6, 142−158

2.5. Products' Characterization

The rheological study was performed using a TA Instruments AR-G2 rheometer. The rheological profile of all synthesized products with an increasing temperature was measured. The compounds were measured at the following conditions: 500 μL quantity of sample, the Peltier platform and cone−plate geometry (40 mm, 2° angle), shear rate of 10 s^{-1}, and temperature ramp from 25 to 50 °C. The Arrhenian plot was formulated as follows (eq 3):[41]

$$\ln \eta = \frac{E_\eta}{R} \cdot \frac{1}{T} + \ln \eta_\infty \tag{3}$$

where the dependence of apparent viscosity $\ln(\eta)$ (−) on the reverse value of temperature $1/T$ (K^{-1}) is constructed. We can obtain the flow activation energy E_η (J/mol) from the slope by multiplying it by the universal gas constant R (J/(mol·K)). Also, we can extract the infinite-temperature viscosity η_∞ (Pa·s) from the y intercept by applying the exponential operation.

The products' solubility was investigated according to calculated RED values (according to Hansen's solubility theory).[42] These were calculated for each compound used in the solubility investigation (the calculation is described in the Supporting Information). According to the theory, the solvent is inappropriate for solubilization when the RED value is above 1. The medium should be a suitable solvent when RED reaches a value below 1. The investigation involved homogenization of the synthesized products with water. The calculated RED parameters were experimentally verified by the following method: 3 g of compound was added to 3 g of water. The mixture was mixed vigorously for 5 min and left at laboratory temperature for 1 day. The results of the solubility experiment were illustrated.

Differential scanning calorimetry (DSC) verified the compounds' curability. The synthesized molecules were mixed with Luperox DI, *tert*-butyl peroxide as thermoinitiator (in 1% w/w quantity to precursor). The mixtures were placed in aluminum pans (10−15 mg) and hermetically sealed. A DSC 2500 model from TA Instruments (New Castle, DE, USA) was used for the analyses. Four different heating scans were performed on each sample from temperatures of 30 to 180 °C with differing temperature ramps: 5, 10, 15, and 20 °C/min. We applied Kissinger's reactivity theory introduced in eq 4:[43]

$$\ln\left(\frac{\beta}{T_p^{\,2}}\right) = \ln\left(\frac{AR}{E_a}\right) - \frac{E_a}{R} \cdot \frac{1}{T_p} \tag{4}$$

where β is the heating rate (°C/min), T_p is the exothermic peak temperature (°C), A is the pre-exponential factor (−), E_a is the activation energy of the reaction (J/mol), and R is the gas constant (J/(mol·K)).

Adhesion on glass and wood was investigated according to the standard ISO 2409. The reactive system (composed of 75 wt % Oil-EA-Met and 25 wt % MGLY/DGLY/TGLY/HEMA) was mixed with the BAPO photoinitiator (1% w/w) and applied to the adherent specimen with dimensions 80 × 25 × 2 mm. The precursor applied quantity was 400 μL. After the dosing, the coated material was covered with a polypropylene lid, allowing the irradiation source to initiate the polymerization. The coated specimens were illuminated by a 405 nm irradiation source exposing 990 mW/m^2 emission power. The curing time was 10 min. The polymer coating on the adherents was investigated via the cross-hatch method (ISO 2409).

The adhesion strength was determined according to ČSN EN 1465 (668510) in a Zwick/Roell 10 kN testing machine under displacement control with a test speed of 1 mm/min. The adhesion area was 25 × 25 mm. The equation determining the adhesion strength ($\sigma_{Adhesion}$) is formulated as follows (eq 5):[45]

$$\sigma_{Adhesion} = \frac{F_{max}}{A} \tag{5}$$

where $\sigma_{Adhesion}$ is the adhesion strength (MPa), F_{MAX} represents the maximum force at adhesion break (N), and A stands for the adhesion area of the specimen (mm^2).

3. RESULTS AND DISCUSSION

3.1. Curable Natural Products' Synthesis

Castor oil and the waste cooking oil contain a significant content of renewable carbon that is used for multiple application fields.[32−34] Modified ricinoleic acid ethanolamide (Oil-EA) was produced by a catalyst-free approach, which represents an efficient and universal way to apply biobased triacylglycerides in the material industry. Next to their potential usage in the polyurethane industry, the hydroxyl functional groups are modifiable by reactive methacrylate groups, ensuring curability of the formed derivative (Oil-EA-Met). This reactive innovative compound possesses two ester bonds along with an amide group, which promises interesting adhesive potential.[46] The activation process involves methacrylic anhydride modifying the hydroxyl groups and generating methacrylic acid as a secondary product. Generated MA is commonly neutralized, washed, or disposed of.[41,48] In this work, a nearly quantitative separation is presented to valorize this reactive compound. Furthermore, the distilled MA served as an activation molecule to generate polar reactive precursors from the valorized cooking oil. The transesterification that was performed led to glycerol generation, which was used as a suitable polyol for Fischer esterification. The separated MA, together with the additional pure MA, ensured the modification toward curable glycerol-derived molecules (MGLY, DGLY, and TGLY). All performed syntheses reached high yields as summarized in Table 1.

Table 1. Summarization of the Synthesis of the Produced Compounds

synthesis			
product	reaction type	purification	yield (%)
Oil-EA	aminolysis	extraction	94.5
Oil-EA-Met	acylation	MA distillation + extraction	92.2
MA	acylation (secondary product)	distillation	88.8
glycerol	transesterification	phase separation + distillation	90.0
MGLY	Fischer esterification	extraction (water phase)	[a]40.2
DGLY	Fischer esterification	extraction (organic phase)	[a]55.2
TGLY	Fischer esterification	water washing	91.2

[a]The yields belong to one reaction mixture (the total yield is their sum).

The synthesized castor-oil-based derivatives were confirmed by ^{1}H NMR, ESI-MS, and FTIR cross-analysis. The complete spectral results are available in the Figure 5 presents the ^{1}H NMR results of the initial castor oil, Oil-EA, and Oil-EA-Met. The changes in the total fatty acid hydrocarbon chains (chemical shift of 1.25−1.75 ppm) confirm the successful aminolysis due to the decrease in the proton number (from 60 protons for castor oil to 20 for Oil-EA). Additionally, the amide functional group's proton presence in the Oil-EA spectrum (3.57−3.66 ppm) and the solid phase product appearance at the laboratory temperature verify the successful Oil-EA synthesis. The following modification by methacrylic

https://doi.org/10.1021/acsengineeringau.5c00084
ACS Eng. Au 2026, 6, 142−158

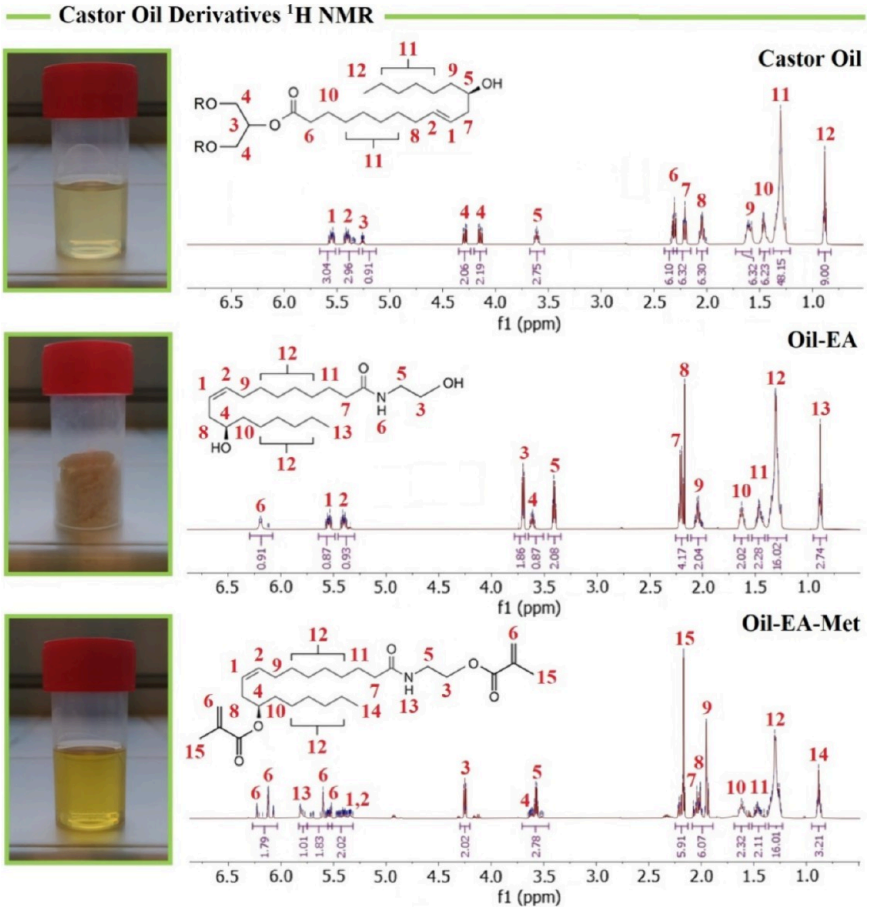

Figure 5. ^{1}H NMR spectra of the castor oil and the synthesized derivatives castor oil ethanolamide (Oil-EA) and castor oil ethanolamide methacrylate (Oil-EA-Met).

anhydride is evident from the typical alkene protons in the chemical shift interval of 5.3−6.3 ppm. A similar ^{1}H NMR outcome was previously published regarding the methacrylation modification of the epoxidized castor oil.[47] Based on the presented cross-analysis, the exact chemical structure of both Oil-EA and Oil-EA-Met was confirmed.

The obtained glycerol from the waste cooking oil was also cross-analyzed, along with the esterified derivatives. Since ^{1}H NMR analysis usually does not provide information regarding the free hydroxyls (as is evident from the presented spectra in Figure 6 and the published literature),[49,50] FTIR and GC-FID contribute to the structure verification. The analyzed ^{1}H NMR glycerol structure corresponds with the published results.[51] All spectra of MGLY, DGLY, and TGLY contain identical signals: the 5.5−6.3 ppm interval indicates the alkene from methacrylate functional groups, the 3.4−4.5 ppm interval refers to the glycerol carbon chain, and the 1.8−2.0 ppm interval signals the presence of terminal methylene groups from the methacrylate group. Next to the exact structural confirmation by ESI-MS and GC-FID (see the Supporting Information), the ^{1}H NMR spectra differ in the analyzed proton ratio of methacrylate functional groups. This result is typical for methacrylate derivatives in the published literature and contributes to the structure confirmation.[48]

The complete FTIR spectra are illustrated in Figure 7; the verification of the presence of free hydroxyl groups is the primary purpose of involving this verification analysis. The wavenumber interval 3700−3100 cm^{-1} provides information regarding the free hydroxyl together with the N−H stretching bonding in the Oil-EA and Oil-EA-Met structure. Since these functional groups cannot be differentiated only by FTIR, the hydroxyl value was measured by titration to quantify the present free hydroxyls in the castor oil and its derivatives. The column graph in Figure 7 illustrates the increasing hydroxyl value of Oil-EA due to ester substitution by an amide terminated by free hydroxyl. After the Oil-EA modification by anhydride, the total hydroxyl value decreases to a negligible 2 mg KOH/g, proving the quantitative modification. The structure is also verified by the disappearance of the ester stretching signal at 1750−1735 cm^{-1} for Oil-EA and its formation for Oil-EA-Met signalizing the methacrylate esters. The glycerol derivative trends are displayed in Figure 7 (right). Continually, the hydroxyl signals at 3700−3100 cm^{-1} decrease with the number of methacrylates as the ester stretching signal (1750−1735 cm^{-1}) and alkene stretching signal (1662−1626 cm^{-1}) increase with the glycerol derivative functionality. The FTIR method is commonly used to monitor the structural changes in the methacrylate derivatives.[41]

3.2. Synthesized Reactive Precursors' Properties

The measured and calculated rheological values and parameters are listed in Table 2. We determined the purity of MGLY, DGLY, and TGLY after the synthesis (Oil-EA-Met was not included due to the GC-FID apparatus limitations connected to the Oil-EA-Met nonvolatility). The purities reached 83.4% for MGLY, 82.2% for DGLY, and 91.1% for TGLY. MGLY and DGLY contain impurities due to the LLE

https://doi.org/10.1021/acsengineeringau.5c00084
ACS Eng. Au 2026, 6, 142−158

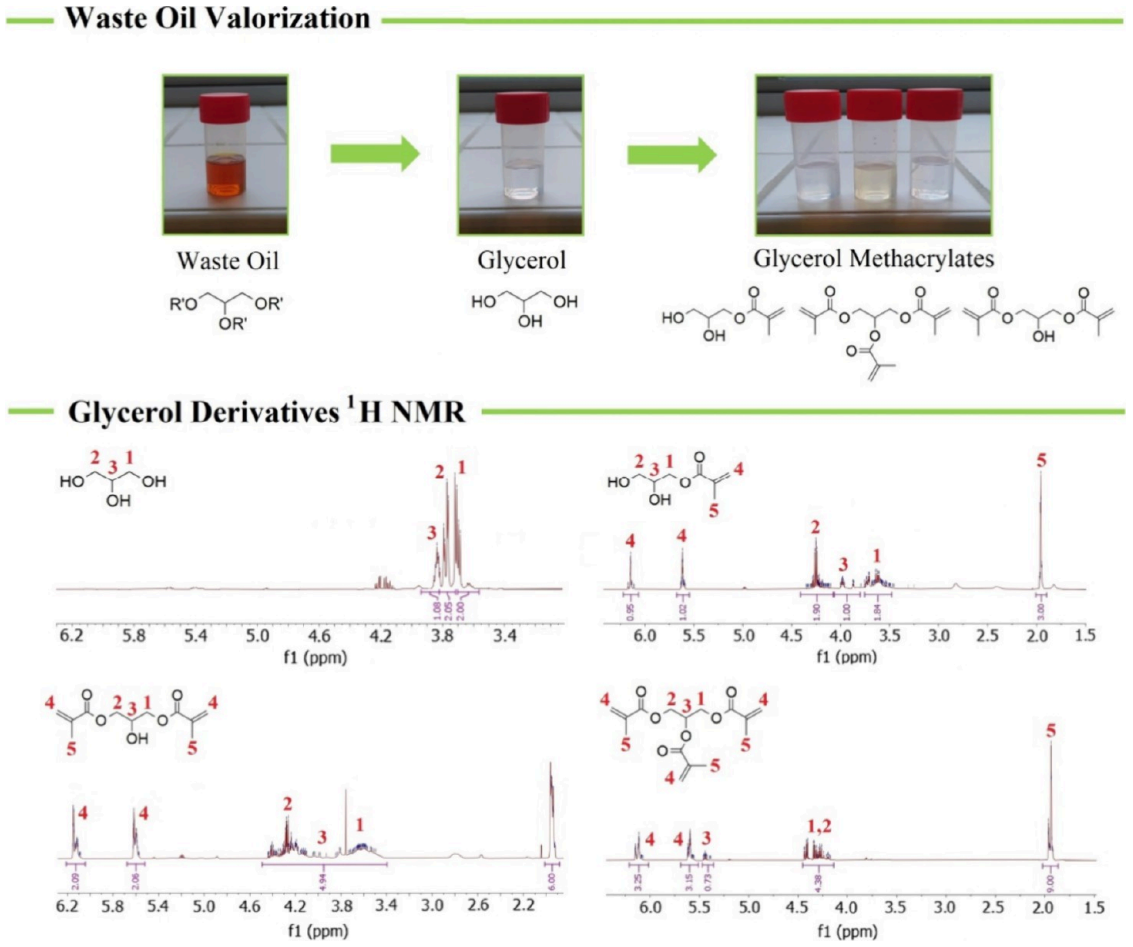

Figure 6. ^{1}H NMR spectra of the synthesized glycerol and the glycerol derivatives glycerol monomethacrylate (MGLY), dimethacrylate (DGLY), and trimethacrylate (TGLY).

process. TGLY reached the highest purity, while the residual MA remained in the precursor. The intermolecular force formation primarily determines the exhibited flow characteristics, which are mainly connected to the compound's functional group composition and total molecular weight.[53] The decreasing viscosity (at 30 °C) corresponds mainly with the remaining free hydroxyl groups within the measured compound's structure. MGLY possesses the highest flow activation energy (E_η = 56.1 kJ/mol) due to the total two free hydroxyl groups within its structure. DGLY exhibits an almost identical flow activation energy (E_η = 54.3 kJ/mol), which corresponds with the rising total molecular weight of the DGLY molecule. The free hydroxyl group is absent in the cases of Oil-EA-Met and TGLY. However, Oil-EA-Met possesses a free amide N−H stretching bond, which contributes to the overall compound's flow activation energy (E_η = 40.4 kJ/mol) together with the highest molecular weight of Oil-EA-Met from all measured molecules. TGLY exhibited the least flow activation energy of all measured glycerol derivatives (E_η = 32.6 kJ/mol) due to the absence of free hydroxyl groups.

The synthesized molecules' reactivity study is illustrated numerically in Table 2 and graphically in Figure 8. The results uncover that the number of free hydroxyls increases the reactivity of the precursor (decreases the polymerization activation energy E_a). Therefore, MGLY achieved the lowest E_a of all of the investigated compounds (E_a = 68.2 kJ/mol). Then, DGLY reached a higher activation energy, as its free hydroxyl content is one functional group (E_a = 81.6 kJ/mol). The least reactive precursors are Oil-EA-Met and TGLY, lacking any free hydroxyl group. These outcomes were previously observed in the published literature, and the positive effect of −OH groups has been described.[58−60] Based on this study, MGLY and DGLY can increase the polymerization reactivity in Oil-EA-Met-based precursor systems and boost the photocuring process, forming the eventual adhesive.

The water solubility of the studied products is essential to their purification after the synthesis, and the overall hydrophilic character also contributes to the potential adhesion performance due to the total content of polar functional groups. The calculated water miscibility according to Hansen's theory is summarized in Table 3. The highest RED value (the least water miscibility) is seen with Oil-EA-Met due to its hydrophobic character enhanced through a long saturated nonpolar hydrocarbon backbone and the total absence of free hydroxyls. TGLY exhibited a RED value of 1.79, which also refers to negligible miscibility with water. This glycerol derivative does not contain any free hydroxyl, similar to Oil-EA-Met. DGLY's RED value reached 1.38, which signaled a higher affinity to water. However, unlimited miscibility cannot be reached with RED values above 1; therefore, DGLY could not be solubilized even with one free hydroxyl in the molecular structure. MGLY's RED level achieved a value of 0.92, which ensures this compound's solubility in water. This calculated

https://doi.org/10.1021/acsengineeringau.5c00084
ACS Eng. Au 2026, 6, 142−158

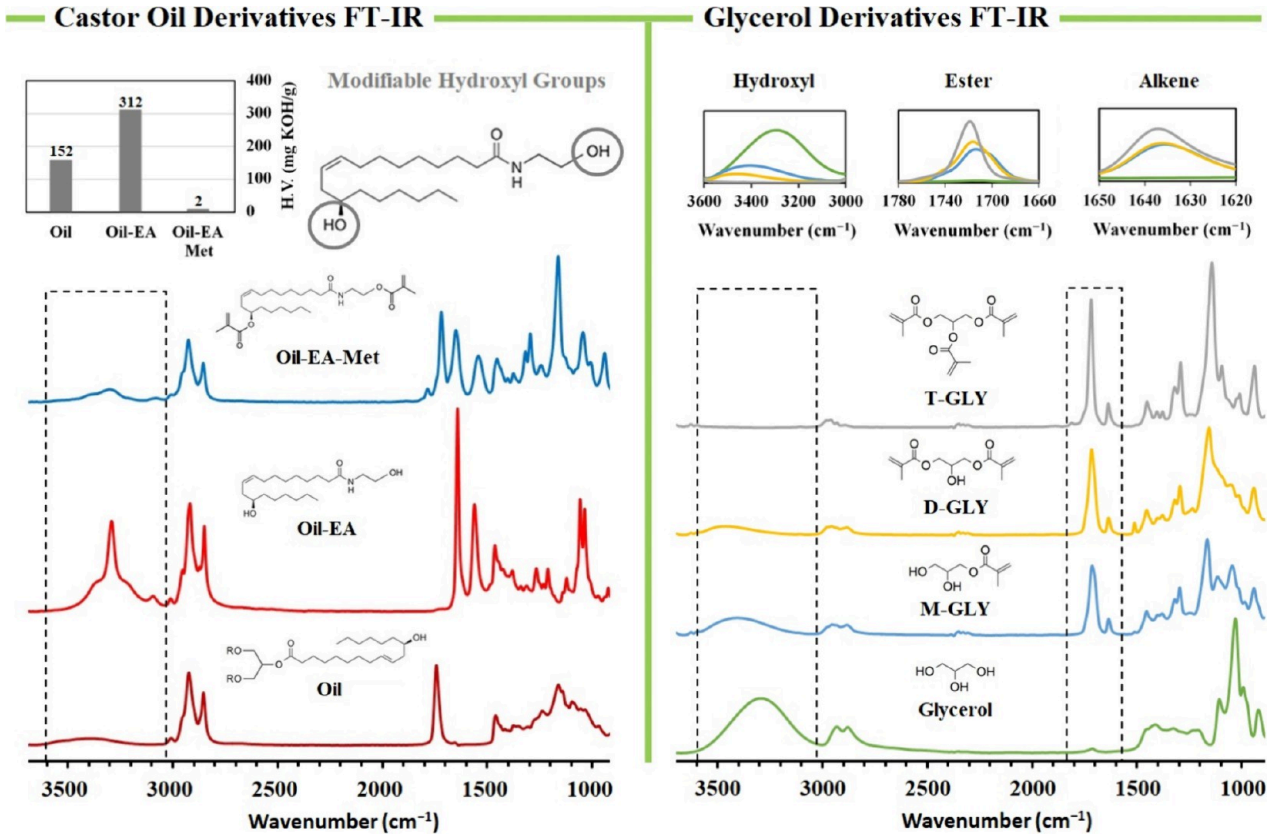

Figure 7. FTIR analysis of the synthesized castor oil and waste cooking oil modified products.

Table 2. Summarization of the Synthesized Products' Rheology, Calculated Reactivity Parameters, and Purity Values

	rheology				reactivity			purity
mixture	$\eta_{30\ °C}$ (mPa·s)	η_{∞} (mPa·s)	E_{η} (kJ/mol)	R^2	E_a (kJ/mol)	ln(A)(−)	R^2	GC-FID value (%)
Oil-EA-Met	191	$1.84 \cdot 10^{-6}$	40.4	0.99	131.8	37.88	0.99	
MGLY	479	$9.31 \cdot 10^{-11}$	56.1	0.99	68.2	19.05	0.98	83.4
DGLY	492	$1.96 \cdot 10^{-10}$	54.3	0.99	81.6	21.7	0.96	82.2
TGLY	14	$3.01 \cdot 10^{-8}$	32.6	0.91	149.2	44.04	0.96	91.1

outcome reflects the two present free hydroxyl groups within MGLY's structure. All calculated predictions were experimentally verified, and the water miscibility (compared with the commercial standard HEMA)[52] results are illustrated in Figure 8.

3.3. Cured Thermosets' Characterization

We formulated five curable systems involving the synthesized precursors. The experimentally investigated cured thermoset-forming solutions comprised Oil-EA-Met as the main system and 25 wt % of each synthesized glycerol derivative (MGLY, DGLY, and TGLY) and the reference (HEMA). The prepared reactive precursors were cured and investigated by real-time FTIR, TGA, DMA, and the flexural test to obtain a complex characterization profile. The FTIR analysis provided information regarding the molecular structure of the formed thermosets and also uncovered the in-time structural changes during the polymerization. The graphs in the Supporting Information (Figures S26−S30) uncover that the molecular structure of the cured thermosets is similar to the uncured precursors except for the C═C bending signal at 840−790 cm^{-1} (indicating the successful polymerization). Both the cured and uncured Oil-EA-Met contain amide H−N bonding (as the FTIR results confirm), while HEMA, MGLY, and DGLY increased the polar character due to the vacant O−H groups. These two groups primarily affected the adhesion performance.[61,62]

We performed the real-time FTIR analysis of the photocuring process (see Figure 9) to fully describe the polymerization process during the irradiation exposure. We calculated the conversion value following the previously published approaches.[63,64] The investigated C═C signal was changed from stretching (1662−1626 cm^{-1}) to bending (840−790 cm^{-1}) due to the presence of amide functional groups. Except for the 100% Oil-EA-Met system, all the cured thermosets reached complete conversion after 10 min of curing. The pure Oil-EA-Met completely polymerized after 20 min. The highest conversion was reached by Oil-EA-Met systems with HEMA (99.4%) and MGLY (99.9%). Based on the results, the system containing DGLY reached the fastest conversion rate (achieving 92.2% conversion after 2 min), while the final degree of cure after 20 min reached nearly a similar value (95.1%) to the multifunctional TGLY-based systems (96.6%). This outcome is probably a combination of the high reactivity (discovered by DSC investigation) and the highest functionality (DGLY contains two polymerizable methacrylate groups).

https://doi.org/10.1021/acsengineeringau.5c00084
ACS Eng. Au 2026, 6, 142−158

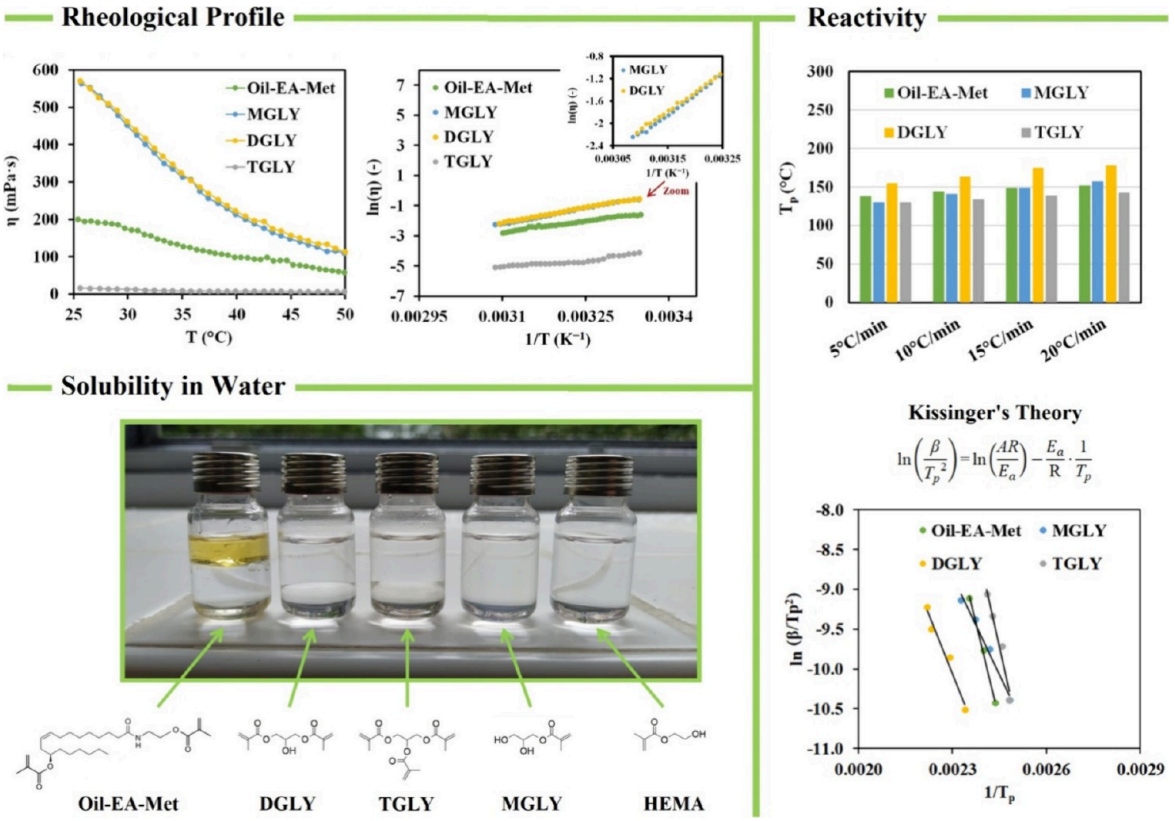

Figure 8. Graphical results of the performed rheological study, including Arrhenius graphical interpretation (top). The experimental water solubility results of the synthesized curable products (bottom). The reactivity investigation results from DSC (side).

Table 3. Calculated Miscibility Interaction Parameters according to Hansen's Theory

	miscibility					
compound	dispersion forces δ_d $(MJ/m^3)^{1/2}$	polar (Keesom) forces δ_p $(MJ/m^3)^{1/2}$	hydrogen bonding forces δ_h $(MJ/m^3)^{1/2}$	forces total δ_{total} $(MJ/m^3)^{1/2}$	RED (−)	water miscibility
Oil-EA-Met	16.80	2.69	6.38	18.17	2.11	×
MGLY	18.46	6.84	19.34	27.59	0.92	√
DGLY	17.82	4.49	13.37	22.73	1.38	×
TGLY	17.51	3.33	9.08	20	1.79	×
[a]water	15.50	16.00	42.30	47.81		

[a]Solubility parameters of water were obtained from the literature.[54]

On the other hand, the additives with a single polymerizable group reached the highest observable conversions. This phenomenon was observable in the literature.[65] Primarily, all the synthesized and formulated systems were completely polymerized after 20 min of photocuring. Moreover, the polymerized layer in the adhesive composition was around 100 μm thick, while the photocuring process was investigated in the 1000 μm layer. Therefore, the complete polymerization was assured in the adhesives.

Figure 10 shows the results of the DMA performed to investigate thermomechanical properties of the composed and formed thermosets, primarily the storage modulus (E') and the glass transition temperature (T_g). The measured values are also listed in Table 4. As the graphs reveal, the 100% Oil-EA-Met thermoset reached the lowest storage modulus at 30 °C (111 MPa) and T_g (47.7 °C). The HEMA-containing system reached higher thermomechanical parameters ($E'_{30°C}$ = 417 MPa and T_g = 65.8 °C). All three systems containing glycerol derivatives (75% Oil-EA-Met with 25% MGLY/DGLY/TGLY) reached very similar storage moduli at 30 °C ($E'_{30°C}$ reached between 770 and 790 MPa), and the glass transition temperature increased with the functionality (T_g of the MGLY system reached 84.4 °C, that of DGLY was 84.5 °C, and that of the TGLY-containing system achieved 86.9 °C). The glycerol-derivative-containing systems reached the highest thermomechanical properties that were expected in the case of DGLY and TGLY due to a higher functionality.[66] Strangely, the MGLY-containing system exhibited high thermomechanical properties despite the monofunctional structure comparable to HEMA's. Based on these findings, MGLY might combine a highly polar structure, which empowers the adhesion while exhibiting an exceptional thermomechanical character compared to its commercial competitor.

The graphical results of the TGA analysis are illustrated in Figure 10, and the numerical values are summarized in Table 4. The performed measurements primarily served to uncover the heat resistance of the formed thermoset. We applied the heat-resistance calculation (T_s) as was previously presented in the

https://doi.org/10.1021/acsengineeringau.5c00084
ACS Eng. Au 2026, 6, 142−158

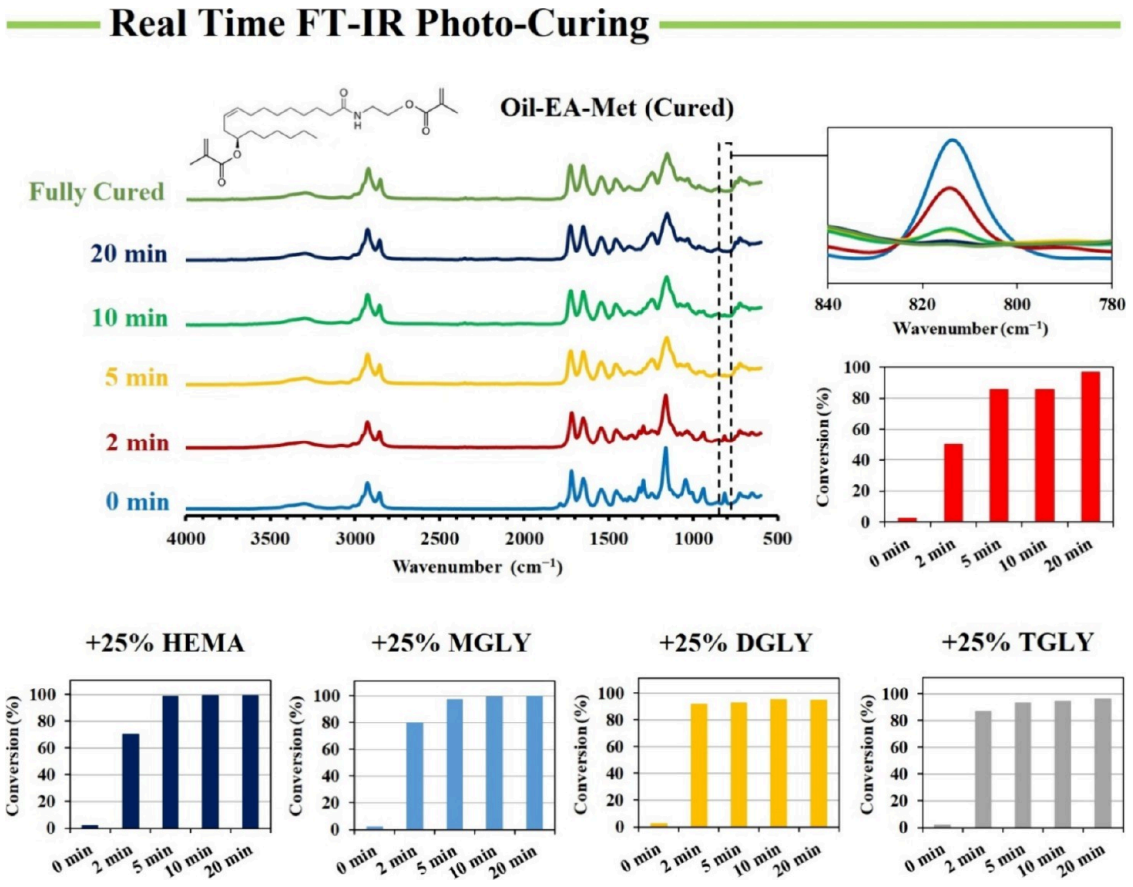

Figure 9. Real-time FTIR analysis of the photocuring process on the formulated thermoset precursors used for the proposed adhesives. The upper overlay signals belong to the 100% Oil-EA-Met system, while the bottom four graphs describe the photocuring of the formulated systems containing 25% of the synthesized additives (MGLY, DGLY, and TGLY) and the reference (HEMA).

published papers.[67,68] The results uncovered that the pure 100% Oil-EA-Met system reached the lowest T_s value of 147.3 °C, while the TGLY-containing system outperformed the rest with a T_s of 164.0 °C. The highest value achieved by the TGLY content is probably a consequence of the highest cross-linked molecular structure by a three-functional monomer, while the absence of free hydroxyls may increase the thermal stability of the thermoset. As the graph in Figure 10c displays, the systems containing glycerol functional derivatives reached considerably higher thermal stability primarily between 350 and 450 °C. Presumably, the glycerol ester structure might be more thermally stable than the ethylene glycol structure (in HEMA) and the amide bonding in the pure Oil-EA-Met.[69] Generally, the glycerol derivatives' content increased the overall thermal stability of the thermoset.

In addition to the DMA investigation providing thermomechanical characteristics, we included flexural tests in the characterization portfolio. The summarized results are displayed in Figure 11, and the complete stress−strain curves are presented in the Supporting Information. The flexural tests correspond with the DMA analysis. The pure Oil-EA-Met system exhibited the highest flexibility (reaching the maximum measured strain of 8.51 ± 0.54%) and the lowest flexural modulus (115 ± 15 MPa) and strength (7.0 ± 0.4 MPa). The addition of HEMA increased the modulus (770 ± 30 MPa) and strength (35.7 ± 1.2 MPa), while the maximum strain remained comparable to the pure Oil-EA-Met (8.25 ± 0.47%). As the functionality of the glycerol derivatives increased, the modulus rose from 1480 ± 36 MPa for the MGLY-containing system to 1689 ± 40 MPa for TGLY involving a thermoset. The flexural strength of all glycerol-derivative-containing systems reached between 63.5 ± 2.1 MPa (MGLY) and 68.0 ± 4.4 MPa (both DGLY and TGLY), which is considerably higher than those of both the pure oil system and the HEMA-containing thermoset. With glycerol's functionality, the maximum strain decreased (MGLY reached 6.77 ± 0.84%, DGLY achieved 6.43 ± 1.02%, and TGLY exhibited 5.09 ± 0.77%), which is in correspondence with the increasing rigidity uncovered by DMA. The mechanical results confirm the previously discussed findings from the thermomechanical analysis and correspond with the literature investigations focused on varying functional curable additives.[70] Based on all of the combined findings, the glycerol reactive derivatives might represent a competitive alternative to the commercial HEMA monomer in Oil-EA-Met-based curable adhesives.

3.4. Photocured Adhesive Performance

The adhesive-to-adherent compatibility is a crucial parameter determining the eventual connection performance. Polar substrates such as wood and glass contain many electronegative functional groups, ensuring a highly hydrophilic character.[9−12] According to the molecular structure and the investigated water miscibility, the highly polar precursors MGLY and DGLY are expected to increase Oil-EA-Met's hydrophilic character and improve the adhesion toward the selected adherents. The coating adhesion evaluated by the ISO 2049 norm for wood and glass substrates is illustrated in Figure

https://doi.org/10.1021/acsengineeringau.5c00084
ACS Eng. Au 2026, 6, 142−158

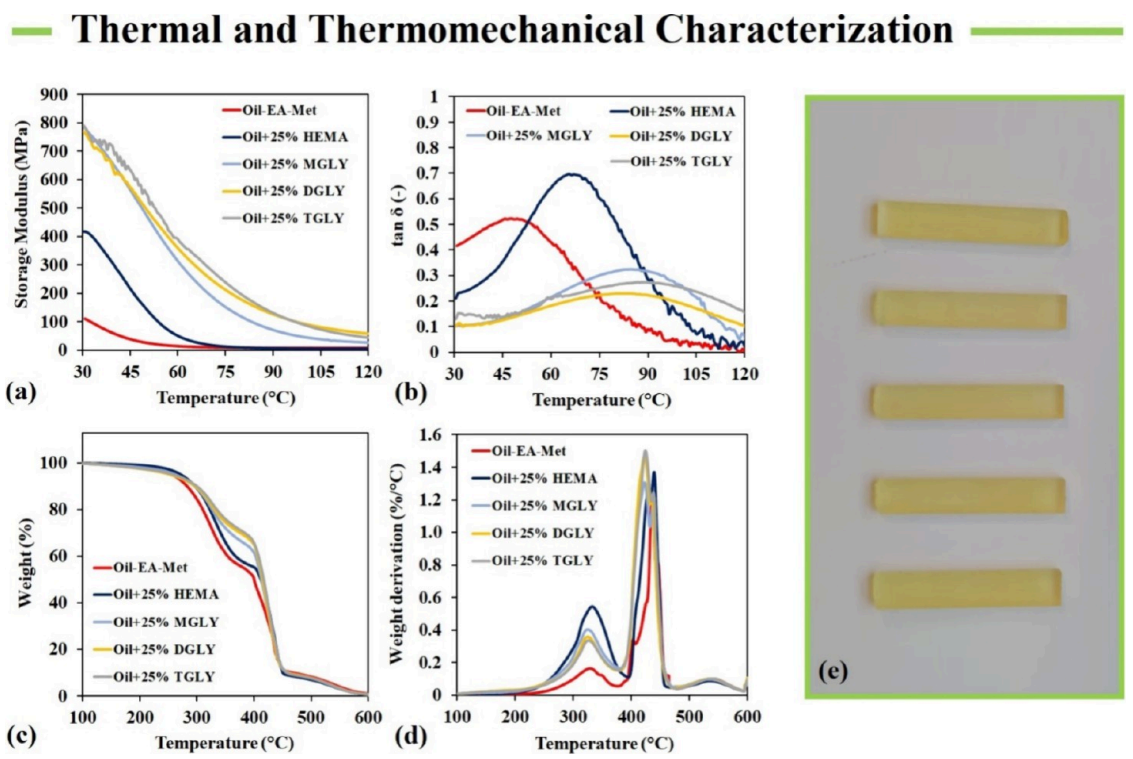

Figure 10. Results of the thermal and thermomechanical characterization. (a) The storage modulus dependence on the temperature ramp. (b) The obtained tan δ curves. (c) The TGA weight loss curves. (d) The TGA-derived weight loss curves. (e) The specimens used for DMA and TGA investigation.

Table 4. Results of the TGA and DMA Analysis

	DMA			TGA		
cured thermoset	$E'_{30°C}$ (MPa)	$E''_{30°C}$ (MPa)	T_g (°C)	T_5 (°C)	T_{30}(°C)	T_s(°C)
Oil-EA-Met	111	46	47.7	257.1	329.8	147.3
25% HEMA	417	98	65.8	272.7	341.8	153.9
25% MGLY	786	80	84.4	263.0	358.9	157.1
25% DGLY	769	82	84.5	254.2	376.4	160.5
25% TGLY	790	109	86.9	260.2	384.4	164.0

12, together with the photos of particular experimentally tested specimens.

The results displayed in Figure 12 confirmed that MGLY and DGLY had a positive effect on adhesion toward wood substrate. The pure Oil-EA-Met thermoset reached ISO 2049 rating level 3, while the performance rating rose to level 5 with 25% MGLY and DGLY in the cured structure. This outcome is directly connected to the higher hydrophilic character of both glycerol derivatives. Strangely, the cured Oil-EA-Met thermoset with 25% HEMA reached a wood adhesion level of 3 despite HEMA's hydrophilic character compared to MGLY. This outcome might be a consequence of HEMA's higher rigidity, which has been investigated in other castor oil polyol derivatives for coating applications.[55] The wood coatings based on the pure Oil-EA-Met and the thermoset with 25% TGLY both recorded a level 3 rating, signifying no positive impact on wood coating performance by the highly nonpolar TGLY. The glass coating adhesion performance achieved the best result for MGLY (reached level 5) and HEMA (reached level 1). HEMA's performance with glass adherence was not ideal, especially in the cross area, probably due to the thermoset's rigidity (similar to the wood substrate). The other systems (100% Oil-EA-Met, 25% DGLY, and 25% TGLY) showed no adhesion to glass, resulting in an ISO 2049 rating level 0. The dominating nonpolar character of the Oil-EA-Met and TGLY structure is possibly incompatible with glass material. Strangely, DGLY also recorded insufficient adhesion. These results confirm the possible necessity of water miscibility (signifying high hydrophilic character and surface tension) for efficient glass adhesion.

In the case of PMMA adhesion, the MGLY-containing system recorded the best ISO 2049 rating (level 3). This outcome enhances the second-best performing system, Oil-EA-Met, reaching a level 2 rating, which corresponds with the nonpolar character of the oil-based precursor. Apparently, MGLY possesses an optimal molecular structure to enhance the adhesion toward a nonpolar surface. The other two polar additives, HEMA and DGLY, achieved a level 1 rating, while the TGLY-containing system failed in the PMMA adhesion test (recorded level 0). The results uncover that the balance of the Oil-EA-Met nonpolar character in combination with MGLY achieves sufficient adhesion toward the polymeric hydrophobic substrate, while HEMA and DGLY systems decrease the adhesion. Next to the polar character, the mechanical and thermomechanical characteristics determine this performance.[74] According to the previous tests, TGLY and DGLY cause an increasingly rigid character. On the other hand, HEMA cannot match the glycerol derivatives' performance from the mechanical and thermomechanical standpoint.

The adhesive shear strength is a standard parameter evaluating the application performance in the published literature.[7,56,57] The adhesion strength calculated from the recorded tensile force is graphically illustrated in Figure 13 together with real specimen photos. The results uncovered that the pure Oil-EA-Met and the thermoset with 25% TGLY

https://doi.org/10.1021/acsengineeringau.5c00084
ACS Eng. Au 2026, 6, 142−158

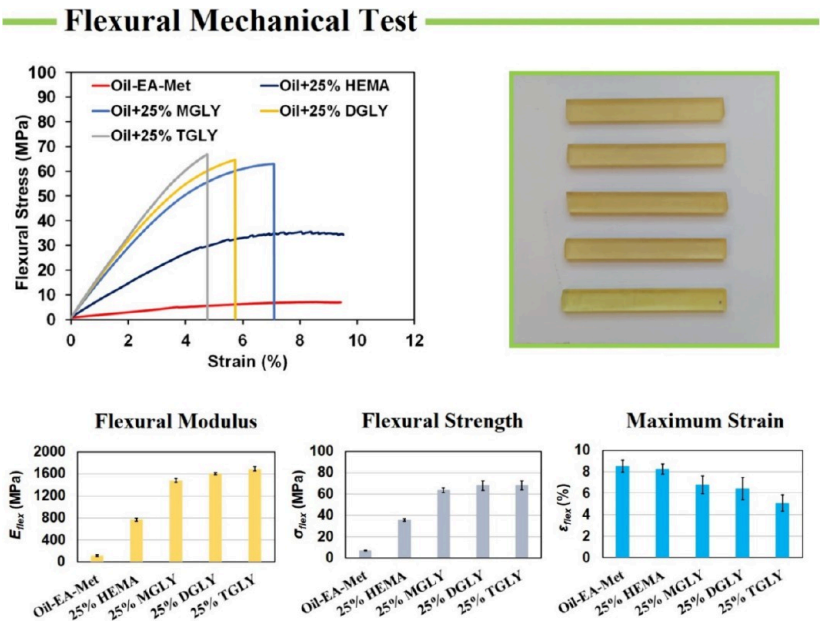

Figure 11. Results of the flexural tests applied to the composed and cured thermoset systems. The testing specimens are displayed in the top right corner. The complete mechanical results are a part of the Supporting Information.

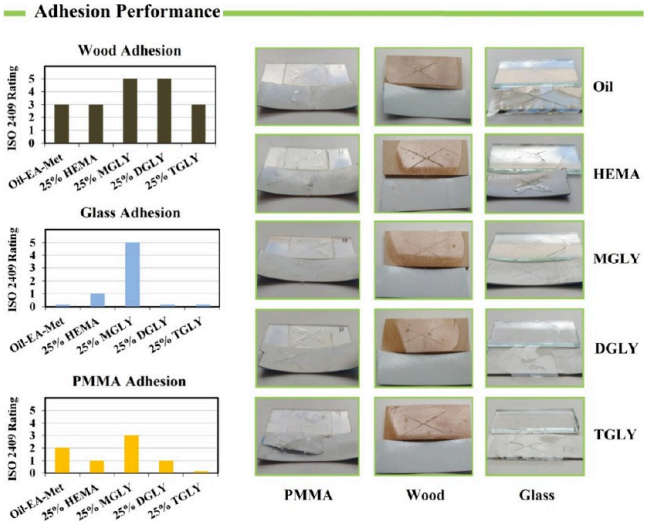

Figure 12. ISO 2049 adhesion rating of the formed and cured thermosets summarized for wood, glass, and poly(methyl methacrylate) (PMMA) adhesion.

achieved practically similar adhesive strength results (around 1000 kPa), signifying no positive effect of TGLY on the castor-oil-based curable adhesive. Additionally, the real specimen photo illustrates the glass adhesion failure of these two samples. This outcome verifies the coating adhesion performance described earlier in Figure 12. On the other hand, the commercial reference 25% HEMA and more polar glycerol derivative thermosets 25% DGLY and 25% MGLY achieved practically similar recorded adhesion shear strength of around 1400 kPa. Although DGLY exhibited insufficient glass adhesion (compared to HEMA and MGLY), its shear strength performance matched those of both water-soluble derivatives. Possibly, the polar character of all three additives in Oil-EA-Met-based thermosets ensures the optimal final adhesion performance. The glass rupture also confirms the exceptional applicability achieved during the tensile test for the HEMA, DGLY, and MGLY systems. Since the material component broke in the measuring process, this result promises an even higher adhesive strength than that measured.

Regarding the PMMA-wood adhesive performance, the overall numerical values recorded by the tensile test are lower compared with the polar glass–wood specimens. Although Oil-EA-Met is a strong hydrophobic oil-derived precursor, the present polar amide functional groups, together with the hydroxyls from most of the additives (HEMA, MGLY, and DGLY), are primarily efficient toward polar substrates. The PMMA–wood adhesion tests (illustrated in Figure 13) uncover that the MGLY-containing system achieved the highest adhesion strength toward the nonpolar PMMA surface (reaching around 800 MPa). The pure Oil-EA-Met system and DGLY-containing adhesive had the second-best adhesion strength (around 640 MPa). The HEMA-containing system recorded 530 MPa of strength, while the TGLY-involving system performed the worst, reaching only 380 MPa of adhesion lap shear strength. This investigation confirmed that MGLY can enhance both polar and nonpolar adhesion provided by an oil-derived photocurable precursor. In the case of PMMA–wood adhesion performance, the commercial HEMA's results were outperformed even by the DGLY additive.

From the long-term adhesion standpoint, the photocurable adhesives decrease their properties tremendously due to their polar molecular structure. The adhesion aging issues were investigated in the literature previously and should be taken into account in an application.[74] The calculated adhesion strengths match other commercially and experimentally tested high-performing adhesives referenced in the published literature.[7,74] Based on the observed adhesion performance, the water miscibility and total polarity mainly affect the adhesion applicability. Also, the synthesized products from valorized glycerol, MGLY and DGLY, performed similarly to a commercially available additive, HEMA, in the case of polar glass–wood adhesion.

https://doi.org/10.1021/acsengineeringau.5c00084
ACS Eng. Au 2026, 6, 142–158

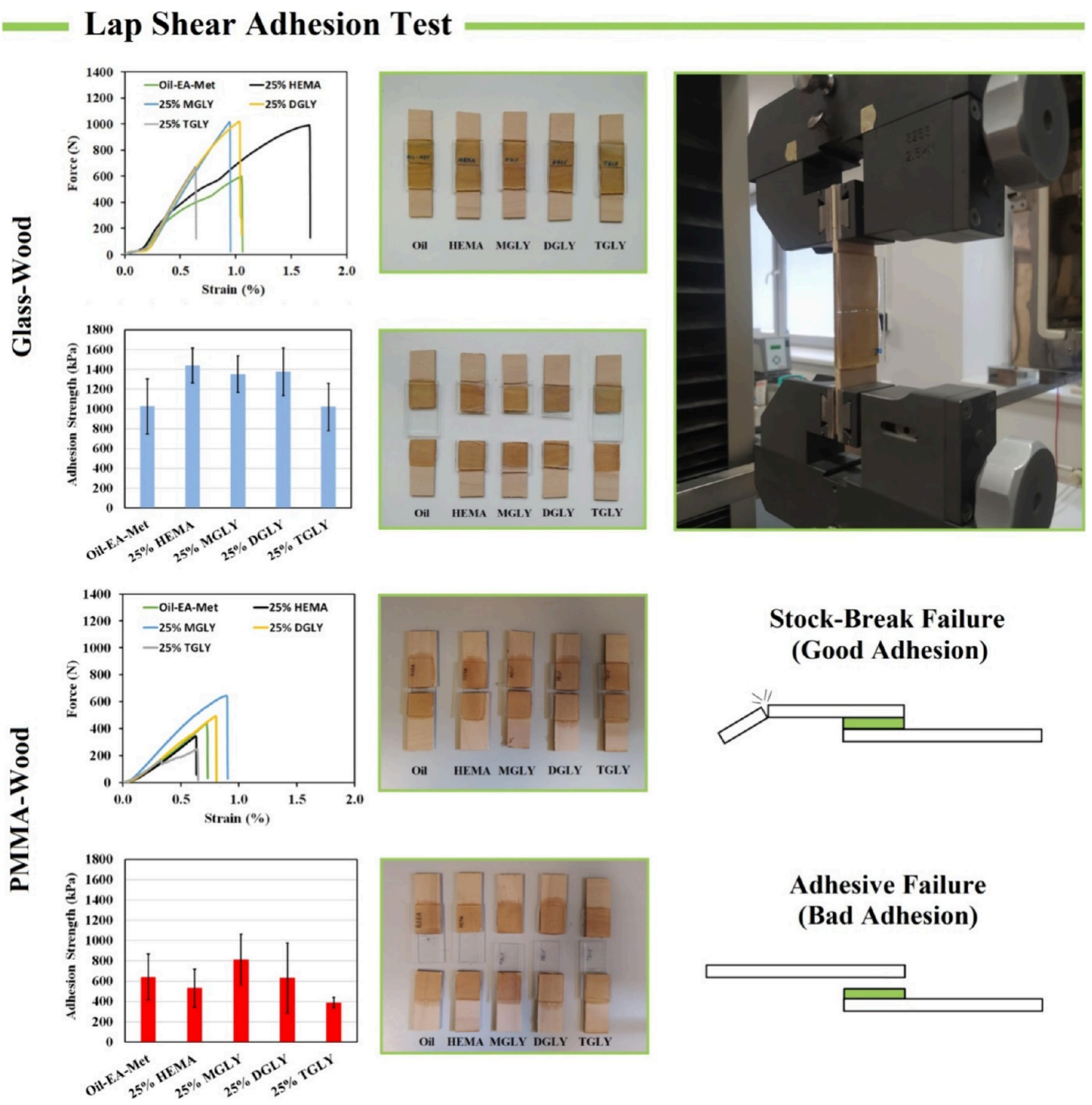

Figure 13. Tensile experimental adhesion application performance investigation of the formulated curable thermosets.

4. CONCLUSIONS

This study investigates a sustainable approach to producing a photocurable adhesive synthesized from natural castor oil and waste cooking oil. An innovative castor oil derivative, ethanolamide methacrylate, was synthesized to form the primary binder precursor. The waste cooking oil was valorized to pure glycerol, which was modified to methacrylate glycerol derivatives, modifying the physical−chemical properties of the produced curable castor oil ethanolamide. All synthesized products from renewable sources were synthesized through a scalable and sustainable approach, resulting in high yields and purities verified by cross-analysis of NMR, ESI-MS, FTIR, and GC-FID. The rheological behavior, water miscibility, and polymerization reactivity were investigated for all curable synthesized products. Eventually, the adhesion performance of the wood and glass coating and the adhesion shear strength were investigated for photocurable mixtures of castor oil ethanolamide methacrylate (Oil-EA-Met) with 25% functional modifier content (glycerol mono/di/trimethacrylate (MGLY, DGLY, and TGLY) and commercial 2-hydroxyethyl methacrylate (HEMA)). Glycerol monomethacrylate (MGLY) achieved the best overall performance in the formed castor-oil-based adhesive. MGLY exhibited a viscosity of 479 mPa·s, a polymerization activation energy of 68.2 kJ/mol, and complete solubility in water. The heat resistance was better than the pure Oil-EA-Met and the commercial HEMA-containing system, reaching 157.1 °C. The storage modulus at 30 °C and the glass transition temperature were superior to the pure-oil-derived

https://doi.org/10.1021/acsengineeringau.5c00084
ACS Eng. Au 2026, 6, 142−158

system and the thermoset with HEMA, achieving $E'_{30°C}$ = 786 MPa and T_g = 84.4 °C. The flexural properties of MGLY combined significantly higher modulus (1689 ± 40 MPa) and strength (63.5 ± 2.1 MPa) than the commercial HEMA-containing system. MGLY reached adhesion coating ISO 2049 rating level 5 (the highest) on a wood adherent and level 5 (the highest) on a glass adherent. The PMMA adhesion reached the highest among the samples measured (level 3). The formulated adhesive containing 75% Oil-EA-Met and 25% MGLY performed similarly to the system with commercial 25% HEMA, reaching approximately 1400 kPa of adhesive shear strength. Also, the PMMA−wood system with MGLY-containing adhesive reached a superior lap shear strength (roughly 800 MPa). The curable adhesive precursor from natural and waste sources performed comparably with the available commercial system.

■ ASSOCIATED CONTENT

Supporting Information

The Supporting Information is available free of charge at https://pubs.acs.org/doi/10.1021/acsengineeringau.5c00084.

Cross-analysis data (Figures S1−S21), additional results of the DSC analysis (Figures S22−S25), a theoretical background to water miscibility, Hansen's theory, cured thermoset structures determined by FTIR (Figures S26−S30), real-time curing FTIR study (Figures S31−S34), additional DMA data (Figure S35), flexural test results (Figure 36-S40), and further data on the adhesion strength measurements (Figures S40−S50) (PDF)

■ AUTHOR INFORMATION

Corresponding Author

Vojtěch Jašek − *Institute of Materials Chemistry, Faculty of Chemistry, Brno University of Technology, Brno 61200, Czech Republic*; orcid.org/0000-0002-8020-4948; Email: xcjasekv@vutbr.cz

Authors

Otakar Bartoš − *Materials Research Centre, Faculty of Chemistry, Brno University of Technology, Brno 612 00, Czech Republic*

Jan Prokeš − *Materials Research Centre, Faculty of Chemistry, Brno University of Technology, Brno 612 00, Czech Republic*

Eliška Kameníková − *Materials Research Centre, Faculty of Chemistry, Brno University of Technology, Brno 612 00, Czech Republic*

Radek Přikryl − *Institute of Materials Chemistry, Faculty of Chemistry, Brno University of Technology, Brno 61200, Czech Republic*

Silvestr Figalla − *Institute of Materials Chemistry, Faculty of Chemistry, Brno University of Technology, Brno 61200, Czech Republic*

Complete contact information is available at: https://pubs.acs.org/10.1021/acsengineeringau.5c00084

Author Contributions

CRediT: **Vojtech Jasek** conceptualization, data curation, formal analysis, investigation, methodology, visualization, writing - original draft, writing - review & editing; **Otakar Bartoš** data curation, formal analysis; **Jan Prokeš** data curation, formal analysis; **Eliška Kameníková** data curation, formal analysis; **Radek Přikryl** resources, supervision, validation; **Silvestr Figalla** resources, supervision, validation.

Notes

The authors declare no competing financial interest.

■ ACKNOWLEDGMENTS

V.J. acknowledges the financial support from the Ministry of Education, Youth, and Sport of the Czech Republic (project FCH-S-25-8836).

■ REFERENCES

(1) Sugita, H.; Itou, K.; Itou, Y.; Wada, N.; Shin-ya Kurita, T. U.; Hirose, Y.; Hatase, K.; Matsumoto, H.; Ichinohe, D. Multi-Acrylate-Based Uv-Curable Dismantlable Adhesives. *Int. J. Adhes. Adhes.* **2021**, *104*, No. 102758.

(2) Azani, M.-R.; Hassanpour, A. Uv-Curable Polymer Nanocomposites: Material Selection, Formulations, And Recent Advances. *Journal of Composites Science* **2024**, *8* (11), 441.

(3) Park, J.; Jin, S.-M.; Mishra, A. K.; Lim, J. A.; Lee, E. Photo-Curable Lacquer Sap Resin Based On Urushiol-Mimicking, Tyrosine-Containing Additive. *Langmuir* **2022**, *38* (32), 10010−10021.

(4) Huang, S.; Wan, Y.; Sun, Y.; Zhang, K.; Ming, X.; Zhu, H.; Zhang, Q.; Zhu, S. Fluorinated Poly(Ionic Liquid) Copolymers As Transparent, Strong, And Versatile Adhesive Materials. *ACS Applied Polymer Materials* **2022**, *4* (5), 3217−3224.

(5) Randall, J. D.; Eyckens, D. J.; Sarlin, E.; Palola, S.; Andersson, G. G.; Yin, Y.; Stojcevski, F.; Henderson, L. C. Mixed Surface Chemistry On Carbon Fibers To Promote Adhesion In Epoxy And Pmma Polymers. *Ind. Eng. Chem. Res.* **2022**, *61* (4), 1615−1623.

(6) Yu, J.; Zheng, S.; You, K.; Mi, Y.; Zhu, W.; Cao, Z. Strong And Flame-Resistant Thermoplastic Polymer Adhesives Based On Multiple Hydrogen Bonding Interactions. *ACS Applied Polymer Materials* **2022**, *4* (5), 3520−3531.

(7) Jamaludin, F. H.; Mohd Yusoff, N. I. S.; Chida, H.; Yang, X.; Wong, T. W.; Zhou, H.; Li, T.; Wang, L.; Goh, P. S.; Ismail, A. F. Photo-Triggered Sustainable Adhesive Based On Itaconic Acid. *ACS Sustainable Chem. Eng.* **2022**, *10* (19), 6389−6401.

(8) Podgórski, R.; Kowalczyk, P.; Leśnowolska-Wnuczek, K.; Dekarz, M.; Kopeć, K.; Młynek, M.; Trzciński, J.; Rybak, E.; Szkop, M.; Ciach, T. Different Strategies For Modifying Polycarbonate Membranes To Control Cell Adhesion. *BioNanoScience* **2025**, *15* (3), 388−403.

(9) Liu, S.; Du, G.; Yang, H.; Su, H.; Ran, X.; Li, J.; Zhang, L.; Gao, W.; Yang, L. Developing High-Performance Cellulose-Based Wood Adhesive With A Cross-Linked Network. *ACS Sustainable Chem. Eng.* **2021**, *9* (49), 16849−16861.

(10) Jašek, V.; Fučík, J.; Bartoš, O.; Figalla, S.; Přikryl, R. Photocurable Oil-Based Thermosets Containing Modifiers From Renewable Sources For Coating Applications. *ACS Polymers Au* **2024**, *4* (6), 527−539.

(11) Huang, S.; Wan, Y.; Ming, X.; Zhou, J.; Zhou, M.; Chen, H.; Zhang, Q.; Zhu, S. Adhering Low Surface Energy Materials Without Surface Pretreatment Via Ion−Dipole Interactions. *ACS Appl. Mater. Interfaces* **2021**, *13* (34), 41112−41119.

(12) Ren, M.; Wu, L.; Yu, B.; Wu, W.; Liu, B.; Xiao, S. Influence Of Adhesive Types On Bonding Defects And Adhesion Performance Of Glass Substrates. *Prog. Org. Coat.* **2024**, *193*, No. 108533.

(13) Pu, B.; Wang, F.; Xu, Y.; Gu, Y.; Liu, L.; Liao, Q. Effect Of Nd2O3 On The Phase Composition, Structure And Aqueous Durability Of Sio2-B2O3-Cao-Na2O-Tio2 Glass-Ceramics. *J. Non-Cryst. Solids* **2024**, *628*, No. 122841.

(14) Sun, C.; Tan, H.; Zhang, Y. Simulating The Pyrolysis Interactions Among Hemicellulose, Cellulose And Lignin In Wood Waste Under Real Conditions To Find The Proper Way To Prepare Bio-Oil. *Renewable Energy* **2023**, *205*, 851−863.

(15) Wibowo, E. S.; Park, B.-D. A Comprehensive Review On Adhesion Interactions Between Formaldehyde−Based Adhesives And Wood Biopolymers On Surface. *J. Adhes.* **2025**, *101*, 1601−1625.
(16) Brandtner-Hafner, M. H. Adhesive bonding systems for construction and building materials. *SOVA Mater. Sci. Technol.* **2022**, *4* (1), 1−9.
(17) Gomez-Lopez, A.; Panchireddy, S.; Grignard, B.; Calvo, I.; Jérôme, C.; Detrembleur, C.; Sardón, H. Poly(Hydroxyurethane) Adhesives And Coatings: State-Of-The-Art And Future Directions. *ACS Sustainable Chem. Eng.* **2021**, *9* (29), 9541−9562.
(18) Yin, X.; Pang, H.; Luo, Y.; Zhang, B. Eco-Friendly Functional Two-Component Flame-Retardant Waterborne Polyurethane Coatings: A Review. *Polym. Chem.* **2021**, *12* (38), 5400−5411.
(19) Cabo, M.; Manoj Narendra, P.; Lee, D.-W.; Yu, R.; Chanthavong, V.; Song, J. I. Improving The Flame Retardancy And Mechanical Properties Of Vinyl Ester Resins Through Maleated Epoxidized Corn Oil/Epoxy Resin Additives For Sustainable Thermoset Composites. *ACS Polym. Au* **2024**, *5* (1), 45−58.
(20) Zhang, Y.; Li, X.; Wei, W.; Liu, X. A Strong Dual-Component Bioadhesive Based On Solventless Thiol-Isocyanate Click Chemistry. *ACS Biomaterials Science & Engineering* **2021**, *7* (7), 3389−3398.
(21) Das, S.; Vasilyev, G.; Martin, P.; Zussman, E. Bioinspired Cationic-Aromatic Copolymer For Strong And Reversible Underwater Adhesion. *ACS Appl. Mater. Interfaces* **2022**, *14* (22), 26287−26294.
(22) Du, Y.; Li, Y.; Li, C.; Xu, R.; Meng, L.; Bai, Y. Optical Adhesives And Screen Sealants For Foldable Displays: Analysis, Progress And Trends. *ACS Appl. Mater. Interfaces* **2025**, *17* (4), 5578−5594.
(23) Unverzagt, L.; Dolynchuk, O.; Lettau, O.; Wischke, C. Characteristics And Challenges Of Poly(Ethylene-Ico/I-Vinyl Acetate) Solution Electrospinning. *ACS Omega* **2024**, *9* (16), 18624−18633.
(24) Li, X.; Wang, Z.; Li, W.; Sun, J. Superstrong Water-Based Supramolecular Adhesives Derived From Poly(Vinyl Alcohol)/Poly(Acrylic Acid) Complexes. *ACS Materials Letters* **2021**, *3* (6), 875−882.
(25) Jeong, Y. J.; Chathuranga, K.; Lee, J. S.; Kim, M. H.; Park, W. H. Sustainable Starch-Extracted Amylose-Rich/Tannic Acid Adhesives With Robust Adhesion Properties On Wood Substrates. *ACS Sustainable Chem. Eng.* **2024**, *12* (38), 14331−14341.
(26) Eissenberger, K.; Ballesteros, A.; De Bisschop, R.; Bugnicourt, E.; Cinelli, P.; Defoin, M.; Demeyer, E.; Fürtauer, S.; Gioia, C.; Gómez, L.; Hornberger, R.; Ißbrücker, C.; Mennella, M.; von Pogrell, H.; Rodriguez-Turienzo, L.; Romano, A.; Rosato, A.; Saile, N.; Schulz, C.; Schwede, K.; Sisti, L.; Spinelli, D.; Sturm, M.; Uyttendaele, W.; Verstichel, S.; Schmid, M. Approaches In Sustainable, Biobased Multilayer Packaging Solutions. *Polymers* **2023**, *15* (5), 1184−1184.
(27) Jašek, V.; Figalla, S. Vegetable Oils For Material Applications − Available Biobased Compounds Seeking Their Utilities. *ACS Polymers Au* **2025**, *5* (2), 105−128.
(28) Li, C.; Hou, D.; Xi, X.; Lei, H.; Tondi, G.; Shi, J.; Du, G. Eco-Friendly Biobased Adhesives Prepared From Different Polyester-Type Glucose With High Cross-Linked Structure. *ACS Sustainable Chem. Eng.* **2024**, *12* (20), 7831−7843.
(29) Lee, S.; Park, J.; Ma, H.; Kim, W.; Song, Y. K.; Lee, D. W.; Noh, S. M.; Yoon, S.-J.; Yang, C. Multifunctional Acrylic Polymers With Enhanced Adhesive Property Serving As Excellent Edge Encapsulant For Stable Optoelectronic Devices. *ACS Appl. Mater. Interfaces* **2024**, *16* (4), 5138−5148.
(30) Glenn, A.; Jensen, A. T.; Machado, F. Isalvia Hispanica/I L. (Chia) Oil As A Potential Renewable Raw Material For The Production Of Air-Dry Alkyd Resins. *ACS Appl. Polym. Mater.* **2021**, *3* (12), 6186−6197.
(31) Frihart, C. R. Chemistry Of Dimer Acid Production From Fatty Acids And The Structure−Property Relationships Of Polyamides Made From These Dimer Acids. *Polymers* **2023**, *15* (16), 3345.
(32) Hayes, G.; Laurel, M.; MacKinnon, D.; Zhao, T.; Houck, H. A.; Becer, C. R. Polymers Without Petrochemicals: Sustainable Routes To Conventional Monomers. *Chem. Rev.* **2022**, *123* (5), 2609−2734.
(33) Xiong, G.; Xiong, W.; Dai, S.; Lin, M.; Xia, G.; Wan, X.; Mu, Y. Fast-Curing Mussel-Inspired Adhesive Derived From Vegetable Oil. *ACS Appl. Bio Mater.* **2021**, *4* (2), 1360−1368.
(34) Lei, H.; Yao, N.; Wang, S.; Fang, X.; Wu, J.; Yang, G.; Hua, Z. Plant Oil-Based Branched Polymer Coatings Enhanced With Nucleobases For Achieving Strong Adhesion And Outstanding Environmental Tolerance. *Chemical Engineering Journal* **2023**, *471*, No. 144602.
(35) Fan, Y.; Shen, H.; Zhang, C.; Chu, X.; Liu, S.; Xing, X.; Tang, E. Fabrication Of Uv-Induced Peelable Adhesives Using Acrylic Copolymers Containing Photo-Initiators And Soybean Oil Based Urethane Acrylate Oligomers. *Int. J. Adhes. Adhes.* **2023**, *126*, No. 103476.
(36) Ho, Y. H.; Parthiban, A.; Thian, M. C.; Ban, Z. H.; Siwayanan, P. Acrylated Biopolymers Derived Via Epoxidation And Subsequent Acrylation Of Vegetable Oils. *International Journal of Polymer Science* **2022**, *2022*, 1−12.
(37) Hua, Z.; Fang, X. Robust Itaconic Acid-Based Polymer Adhesive Nanocomposites Containing Bioinspired Multiple Hydrogen Bonds At The Polymer−Nanofiller Interface. *Macromolecules* **2023**, *56* (19), 8047−8053.
(38) Carrasco-Fernández, M.; López-Martínez, E. I.; Flores-Gallardo, S. G.; Estrada-Moreno, I. A.; Mendoza-Duarte, M. E.; Vega-Rios, A. Innovative Poly(Lactic Acid) Blends: Exploring The Impact Of The Diverse Chemical Architectures From Itaconic Acid. *Polymers* **2024**, *16* (19), 2780−2780.
(39) Afewerki, S.; Edlund, U. Engineering An All-Biobased Solvent- And Styrene-Free Curable Resin. *ACS Polymers Au* **2023**, *3* (6), 447−456.
(40) Wang, F.; Allen, D.; Tian, S.; Oler, E.; Gautam, V.; Greiner, R.; Metz, T. O.; Wishart, D. S. Cfm-Id 4.0 − A Web Server For Accurate Ms-Based Metabolite Identification. *Nucleic Acids Res.* **2022**, *50* (W1), W165−W174.
(41) Liu, W.; Xie, T.; Qiu, R. Biobased Thermosets Prepared From Rigid Isosorbide And Flexible Soybean Oil Derivatives. *ACS Sustainable Chem. Eng.* **2017**, *5* (1), 774−783.
(42) Hansen, C. M. *Hansen Solubility Parameters: A User's Handbook*, 2nd ed. 2007. .
(43) Mashouf Roudsari, G.; Mohanty, A. K.; Misra, M. Study Of The Curing Kinetics Of Epoxy Resins With Biobased Hardener And Epoxidized Soybean Oil. *ACS Sustainable Chem. Eng.* **2014**, *2* (9), 2111−2116.
(44) Nouailhas, H.; Aouf, C.; Le Guerneve, C.; Caillol, S.; Boutevin, B.; Fulcrand, H. Synthesis And Properties Of Biobased Epoxy Resins. Part 1. Glycidylation Of Flavonoids By Epichlorohydrin. *J. Polym. Sci., Part A: Polym. Chem.* **2011**, *49* (10), 2261−2270.
(45) Beber, V. C.; Wolter, N.; Schneider, B.; Koschek, K. Effect Of Aluminium Substrate Thickness On The Lap-Shear Strength Of Adhesively Bonded And Hybrid Riveted-Bonded Joints. *Proceedings of the Institution of Mechanical Engineers, Part E: Journal of Process Mechanical Engineering* **2023**, *237* (3), 607−614.
(46) He, J.; Ding, Y.; Jiang, F.; Wang, Z. Poly(Ester Amide)S Derived From Low-Value Plant Oil As Reusable Low-Temperature Tolerant Adhesives. *Eur. Polym. J.* **2023**, *198*, No. 112387.
(47) Çayli, G.; Gürbüz, D.; Çınarli, A. Characterization And Polymerization Of Epoxidized Methacrylated Castor Oil. *European Journal of Lipid Science and Technology* **2019**, *121* (1), 1700189−1700194.
(48) Badía, A.; Agirre, A.; Barandiaran, M. J.; Leiza, J. R. Removable Biobased Waterborne Pressure-Sensitive Adhesives Containing Mixtures Of Isosorbide Methacrylate Monomers. *Biomacromolecules* **2020**, *21* (11), 4522−4531.
(49) Cseri, L.; Kumar, S.; Palchuber, P.; Szekely, G. Nmr Chemical Shifts Of Emerging Green Solvents, Acids, And Bases For Facile Trace Impurity Analysis. *ACS Sustainable Chem. Eng.* **2023**, *11* (14), 5696−5725.

https://doi.org/10.1021/acsengineeringau.5c00084
ACS Eng. Au 2026, 6, 142−158

(50) Parada Hernandez, N. L.; Bonon, A. J.; Bahú, J. O.; Barbosa, M. I. R.; Wolf Maciel, M. R.; Filho, R. M. Epoxy Monomers Obtained From Castor Oil Using A Toxicity-Free Catalytic System. *J. Mol. Catal. A: Chem.* **2017**, *426*, 550−556.
(51) Trindade Mazala, T.; Costa Viana, M.; Carneiro, G.; Lee Nelson, D.; de Freitas-Marques, M. B.; De Martinis, B. S.; Florêncio, J.; Mazzé, F. M.; da Silva, S. G. D.; Barbosa, S. L. Purification And Use Of Crude Green Glycerol From The Transesterification Of Triglycerides In The Formulation Of An Alcohol Gel Hand Sanitizer. *Sci. Rep.* **2024**, *14* (1), 5510−5510.
(52) *Ataman Chemicals*, 2020. https://www.atamanchemicals.com/hema-2-hydroxyethyl-methacrylate_u27391/
(53) Grayson, J. W.; Evoy, E.; Song, M.; Chu, Y.; Maclean, A.; Nguyen, A.; Upshur, M. A.; Ebrahimi, M.; Chan, C. K.; Geiger, F. M.; Thomson, R. J.; Bertram, A. K. The Effect Of Hydroxyl Functional Groups And Molar Mass On The Viscosity Of Non-Crystalline Organic And Organic−Water Particles. *Atmospheric Chemistry and Physics* **2017**, *17* (13), 8509−8524.
(54) Date, A. A.; Srivastava, D.; Nagarsenker, M. S.; Mulherkar, R.; Panicker, L.; Aswal, V.; Hassan, P. A.; Steiniger, F.; Thamm, J.; Fahr, A. Lecithin-Based Novel Cationic Nanocarriers (Leciplex) I: Fabrication. *Characterization And Evaluation. Nanomedicine* **2011**, *6* (8), 1309−1325.
(55) Shaik, A.; Nehete, K. K.; Shyamroy, S. Effective Studies of bio-derived free radical polymerizable hydroxyl functional macro-monomer for replacement of Hydroxylethyl Methacrylate (HEMA) in acrylic polyols and their polyurethane-urea coatings. *J. Polym. Res.* **2024**, *32* (2), 66−85.
(56) Corigliano, P.; Crupi, V.; Bertagna, S.; Marinò, A. Bio-Based Adhesives For Wooden Boatbuilding. *Journal of Marine Science and Engineering* **2021**, *9* (1), 28.
(57) Chen, S.; Chen, Y.; Wang, Z.; Chen, H.; Fan, D. Renewable Bio-Based Adhesive Fabricated From A Novel Biopolymer And Soy Protein. *RSC Adv.* **2021**, *11* (19), 11724−11731.
(58) Zhang, Y.; Li, Y.; Thakur, V. K.; Wang, L.; Gu, J.; Gao, Z.; Fan, B.; Wu, Q.; Kessler, M. R. Bio-Based Reactive Diluents As Sustainable Replacements For Styrene In Maeso Resin. *RSC Adv.* **2018**, *8* (25), 13780−13788.
(59) Jašek, V.; Fučík, J.; Melčová, V.; Přikryl, R.; Figalla, S. Improvements In The Production Of Isosorbide Monomethacrylate Using A Biobased Catalyst And Liquid−Liquid Extraction Isolation For Modifications Of Oil-Based Resins. *ACS Omega* **2024**, *9* (23), 24728−24738.
(60) Yang, R.; Li, N.; Evans, C. J.; Yang, S.; Zhang, K. Phosphaphenanthrene-Functionalized Benzoxazines Bearing Intramolecularly Hydrogen-Bonded Phenolic Hydroxyl: Synthesis, Structural Characterization, Polymerization Mechanism, And Property Investigation. *Macromolecules* **2023**, *56* (4), 1311−1323.
(61) Kim, K.; Yoo, T.; Lee, J.; Kim, M.; Lee, S.-R.; Kim, G.; Kim, J.; Han, P.; Han, H. The Effects Of Hydroxyl Groups On The Thermal And Optical Properties Of Poly(Amide-Imide)S With High Adhesion For Transparent Films. *Prog. Org. Coat.* **2017**, *112*, 37−43.
(62) Fischer, L.; Strzelczyk, A. K.; Wedler, N.; Kropf, C.; Schmidt, S.; Hartmann, L. Sequence-Defined Positioning Of Amine And Amide Residues To Control Catechol Driven Wet Adhesion. *Chem. Sci.* **2020**, *11* (36), 9919−9924.
(63) Konuray, O.; Salla, J. M.; Morancho, J. M.; Fernández-Francos, X.; García-Alvarez, M.; Ramis, X. Curing Kinetics Of Acrylate-Based And 3D Printable Ipns. *Thermochim. Acta* **2020**, *692*, No. 178754.
(64) Denis, A. B.; Diagone, C. A.; Plepis, A. M. G.; Viana, R. B. Kinetic Parameters During Bis-Gma And Tegdma Monomer Polymerization By Atr-Ftir: The Influence Of Photoinitiator And Light Curing Source. *J. Spectrosc.* **2016**, *2016*, No. 6524901.
(65) Bergoglio, M.; Najmi, Z.; Cochis, A.; Miola, M.; Vernè, E.; Sangermano, M. Uv-Cured Bio-Based Acrylated Soybean Oil Scaffold Reinforced With Bioactive Glasses. *Polymers* **2023**, *15* (20), 4089−4089.
(66) He, Q.; Hu, L.; Huang, Y.; Huang, T.; Zhu, Z.; Li, Y.; Hu, Y.; Yang, Z. Eugenol-Based Multi-Functional Monomer As Reactive Diluent For High Bio-Content Uv-Curable Coatings. *Prog. Org. Coat.* **2025**, *200*, No. 109079.
(67) Zhu, H.; Zhu, Y.; Bao, D.; Pei, L.; Xu, F.; Wang, Z.; Wang, H. Research On Improving The Thermal Conductivity Of Epoxy Resin With Flexible Assisted Rigid Groups. *Chin. J. Polym. Sci.* **2024**, *42* (11), 1845−1854.
(68) Lotos, E.; Dinu, R.; Mihai, M.; Simionescu, B. C.; Mija, A. Development Of Eco-Friendly Thermosetting Resins From Zein And Diglycidyl Ether Of Vanillyl Alcohol. A Step Toward Sustainable Materials. *Chem.-Eur. J.* **2025**, *31* (27), No. e202500624.
(69) Saunoryte, E.; Navaruckienė, A.; Grauželienė, S.; Bridžiuvienė, D.; Raudonienė, V.; Ostrauskaitė, J. Glycerol Acrylate-Based Photopolymers With Antimicrobial And Shape-Memory Properties. *Polymers* **2024**, *16* (6), 862−862.
(70) Grimalt, J.; Frattini, L.; Carreras, P.; Fombuena, V. Optimizing Rheological Performance Of Unsaturated Polyester Resin With Bio-Based Reactive Diluents: A Comprehensive Analysis Of Viscosity And Thermomechanical Properties. *Polym. Test.* **2023**, *129*, No. 108264.
(71) Huang, Q.; Li, Z.; Bao, Z.; Xu, X.; Liu, H.; Zhang, M.; Qing, Y.; Li, X.; Wu, Y. Nature-Derived Adhesives Based On Chitosan And Rosin Acid With High Strength, Flame Retardancy, And Environmental Friendliness. *Green Chem.* **2025**, *27* (39), 12319−12332.
(72) Toth, V.; Hardian, R.; Vovusha, H.; Yang, C.; Szekely, G. Interfacial Polymerization Of Dopamine With Diamines For Ultrastable Janus Nanofiltration Membranes And Adhesives. *Mater. Today* **2025**, *86*, 104−114.
(73) Jiang, Z.; Lv, Q.; Zhao, F.; Pan, B.; Liu, Y.; Song, X.; Li, H.; Wang, Y. A Sustainable Scpl/Scp-Serine-Induced Hydrogel With Ultrafast Gelation, Mechanical Resilience, And Environmental Robustness For Efficient Sand Stabilization. *Journal of Materials Chemistry A* **2025**, *13* (35), 29323.
(74) Jamaludin, F. H.; Mohd Yusoff, N. I. S.; Chida, H.; Yang, X.; Wong, T. W.; Zhou, H.; Li, T.; Wang, L.; Goh, P. S.; Ismail, A. F. Photo-Triggered Sustainable Adhesive Based On Itaconic Acid. *ACS Sustainable Chem. Eng.* **2022**, *10* (19), 6389−6401.

https://doi.org/10.1021/acsengineeringau.5c00084
ACS Eng. Au 2026, 6, 142−158